# Interseed and tissue-composition effects in permanent low dose rate brachytherapy

By
Marie-Joëlle Bertrand

Master's thesis

Medical Physics Unit
Montreal General Hospital
McGill University

Montreal, Quebec, Canada
May 12, 2008

A thesis submitted to McGill University in partial fulfilment of the requirements of the degree of M. Sc. in Medical Physics.

# Table of contents

# Abstract

Permanent Low Dose Rate (LDR) brachytherapy is mostly used for the treatment of prostate cancer and is also used for breast cancer treatment. The dosimetry is made using the TG-43 protocol in which the interseed and the tissue-composition effects are ignored.

The interseed effect is the impact of the presence of the seeds on the dosimetry. By ignoring that effect, the Dose Volume Histogram (DVH) is right-shifted and dose analysis parameters such as the D90 are overestimated.

The tissue-composition effect is due to the presence of materials different from water around the seeds. In prostate tissue, the DVH is right shifted when this effect is ignored and the dosimetry is made using the TG-43 formalism. In breast tissue the DVH is left shifted when the tissue-composition effect is ignored. The tissue-composition effect is more important in breast tissue than in prostate tissue, so that parameters like the D90 are greatly underestimated by doing the dosimetry for a breast permanent LDR brachytherapy treatment using the TG-43 protocol.

# Résumé

La curiethérapie permanente à faible débit de dose est surtout utilisée pour traiter le cancer de la prostate et est aussi utilisée pour le traitement du cancer du sein. La dosimétrie est faite en utilisant le formalisme du TG-43 dans lequel l'effet intergrain et l'effet de composition sont ignorés.

L'effet intergrain est l'impact de la présence des grains sur la dosimétrie. Quand cet effet est ignoré, le DVH (Dose Volume Histogram) est décalé vers la droite et les paramètres dosimétriques comme la D90 sont surestimés.

L'effet de composition est dû à la présence de matériel différent de l'eau autour des grains. Dans du tissus prostatique, le DVH est décalé vers la droite quand cet effet est ignoré et que la dosimétrie est faite avec le protocole TG-43. Dans le sein, le DVH est décalé vers la gauche quand l'effet de composition est ignoré. L'effet de composition est plus important pour le sein que pour la prostate. Conséquemment, les paramètres comme la D90 sont grandement sous-estimés en faisant la dosimétrie pour un traitement du sein en curiethérapie permanente à faible débit avec le protocole TG-43.

# Acknowledgements

First, I would like to thank my supervisor, Brigitte Reniers for her help and support during my research. I would also like to thank my co-supervisor, Frank Verhaegen for his patience and for the good suggestions he gave me.

I also want to thank my fellow students and all the staff at the McGill MPU.

The completion of this research would not have been possible without the support and help of the medical physics team at HMR. I particularly thank to Patrice Munger for the help with programming, Maryse Mondat for the radioprotection work and Wieslaw Wierzbicki for welcoming me in the department.

I thank my colleagues at the CSSSC, Hugo Tremblay, Vincent Lalande and Patrice Jones and Brigitte Côté, chief of the radio-oncology department for their understanding.

Thank you to *International Brachytherapy* (IBt) for providing the seeds. Thank you also to the M*inistère de la santé et des services sociaux* (MSSS) for the bursary.

Finally a big thank you to my parents Jocelyne and Michel Bertrand and to my sister Juliane Bertrand for believing in me and supporting me.

# List of figures

# List of tables

# List of symbols and abbreviations

| | |
|---|---|
| CT | Computed tomography |
| d | Distance |
| D | Total dose |
| $\dot{D}_o(r,\theta)$ | Initial dose rate at point (r,θ) |
| D(r,θ) | Dose at point (r,θ) |
| $D_m$(r,θ) | Measured dose at point (r,θ) |
| DVH | Dose volume histogram |
| $D_X$ | Dose given to X% of the volume |
| E | Energy |
| $\overline{E}_{out}$ | Average exiting energy. |
| F(r,θ) | Anistropy function |
| F4 | track length estimate of cell flux tally |
| F6 | energy deposition averaged over a cell tally |
| F8 | Pulse height tally |
| FMCS | Full MC simulation |
| $\dot{K}_{\partial}(d)$ | Air-kerma rate due to photons of energy superior to a cut-off δ |
| g(r) | Radial dose function |
| G(r,θ) | Geometric function |
| H(E) | Heating number |
| HDR | High dose rate |
| OAR | Organ at risk |
| IMRT | Intensity modulated radiotherapy |
| KERMA | Kinetic energy released in media |
| L | Active length of the seed |
| LDR | Low dose rate |
| LSKS | Line source dose kernel superposition |
| m | Mass |
| MCP | MC with realistic prostate tissues |
| MCW | MC with water prostate |
| mPD | minimum peripheral dose |
| $N(\vec{r},E,t)$ | Particle density |
| netOD | Net optical density |
| $p_i$(E) | Probability of reaction i |
| PSKS | Point source dose kernel superposition |
| PTV | planing target volume |
| r | Distance from the longitudinal axis of a seed |
| RCF | Radiochromic film |
| $S_k$ | Air-kerma strenght |
| SMC | Superposition of MC |
| t | Actual time of the experiment |
| $t_{eff}$ | Effective time of the experiment |
| $T_l$ | Track lenght |

| | |
|---|---|
| TLD | Thermo-luminescent dosimeter |
| TRUS | Transrectal ultrasound |
| U | Unit of $S_k$ |
| V | Volume |
| $V_X$ | Volume receiving X% of the prescribed dose |
| W | Particle weight |
| WAFAC | Wide-Angle Free-Air Chamber |
| $W_s$ | Source weight |
| δ | Cut-off energy |
| θ | Angle from the transverse axis of a seed |
| λ | Decay constant |
| Λ | Dose rate constant |
| $\rho_a$ | Atomic density |
| $\rho_g$ | Physical density |
| $\Phi(\vec{r},E,t)$ | Particle flux |
| $v$ | Particle velocity |
| $\sigma_T(E)$ | Total cross section |

# Chapter 1. Introduction

This work is about permanent low dose rate (LDR) brachytherapy. More precisely, this study is about interseed and tissue composition effects in permanent LDR brachytherapy.

Permanent LDR brachytherapy is generally used for the treatment of prostate cancer. Recently, the application of permanent LDR brachytherapy for the treatment of breast cancer has also been developed.

## 1.1. Brachytherapy vs external beam

*Radiotherapy* is the treatment of a disease (commonly cancer) with radiation. Such a treatment can be made using radiation sources that are positioned either outside or at a certain distance from the patient (*external beam therapy*) or radiation sources that are positioned inside or immediately close to the patient (*Brachytherapy*). The use of brachytherapy has the particularity to give the dose directly to the tumor while limiting the dose to surrounding tissues (the dose falloff is very steep). Some advantages and disadvantages of brachytherapy compared to external beam therapy are discussed in TG-56[1] :

> Compared to conventional external beam therapy, the physical advantages of brachytherapy results from a superior localization of dose to the tumor volume. On the other hand, the dose gradients around an implant and dose heterogeneity within an implant are much higher than dose in external beam radiotherapy.

Some practical considerations, like the possibility in brachytherapy to give more dose to the tumor with less complications to normal tissues[2] and some brachytherapy techniques that permits a single fraction treatment might also be taken into account to favour brachytherapy. However the tumor must be localised in brachytherapy, while external beam permit to give dose to an extended target. Isodoses for radiotherapy and brachytherapy are shown in figures 1.1 and 1.2.

## 1.2. Historic

Brachytherapy was developed shortly after Becquerel discovered natural radioactivity in 1896 and the Curies discovered radium in 1898. In 1901, Pierre Curie

suggested the insertion of a tube of radium in a tumor to a doctor at St-Louis Hospital, in Paris. In 1903, Alexander Graham Bell made a similar suggestion in a letter to the editor of *Archives Roentgen Ray.* Experiments quickly showed that the insertion of radioactive material had the effect of shrinking the tumor. Afterloading procedures, using rubber tube as an applicator in which removable sources can be put after the application, were performed as soon as 1905 by Dr. Robert Abbe[3] .

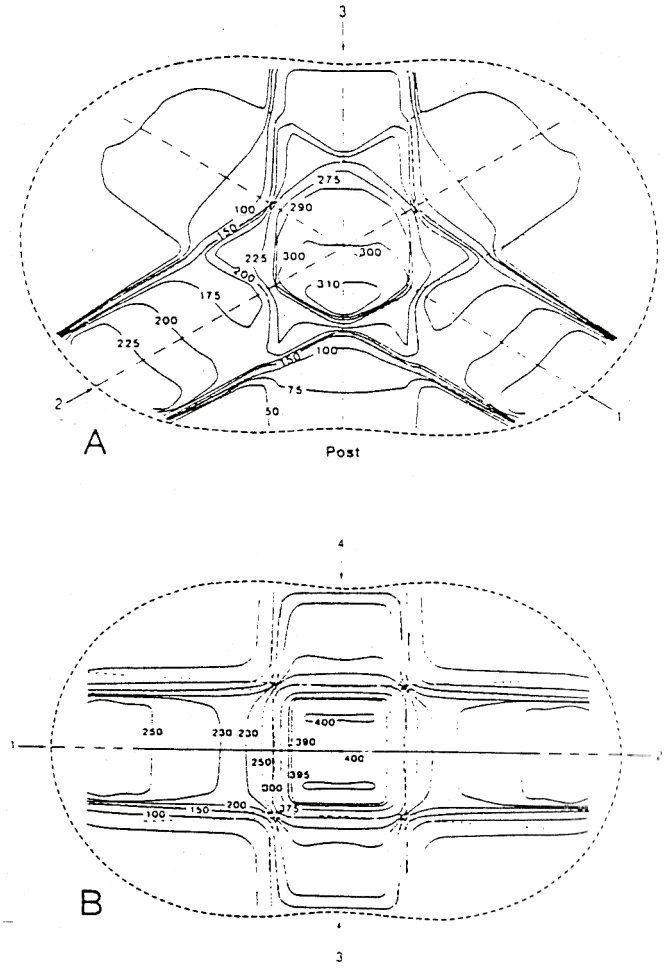


Figure 1.1 : Isodoses for two external plans. a) three field isocentric technique, 8x8 $cm^2$ beams, 4 MV. b) four fields isocentric technique, 8x8 $cm^2$ beams, 10 MV[4].

Dr. Pasteau who inserted $^{226}Ra$ in the prostatic urethra using a cathether[5] reported the first published case of prostate brachytherapy treatment in 1911. The short-term control of the tumor was good, but this technique caused too many complications. In 1917, Barringer implanted $^{226}Ra$ needles in the prostate, using

touch through the rectum as a position guidance[5] The effects were good, but this crude way of guidance was insufficient. To correct that problem some creative techniques were tried, like, in the 1950's, the injection of a solution of colloidal radioactive gold in the prostate by Dr Flocks[6].

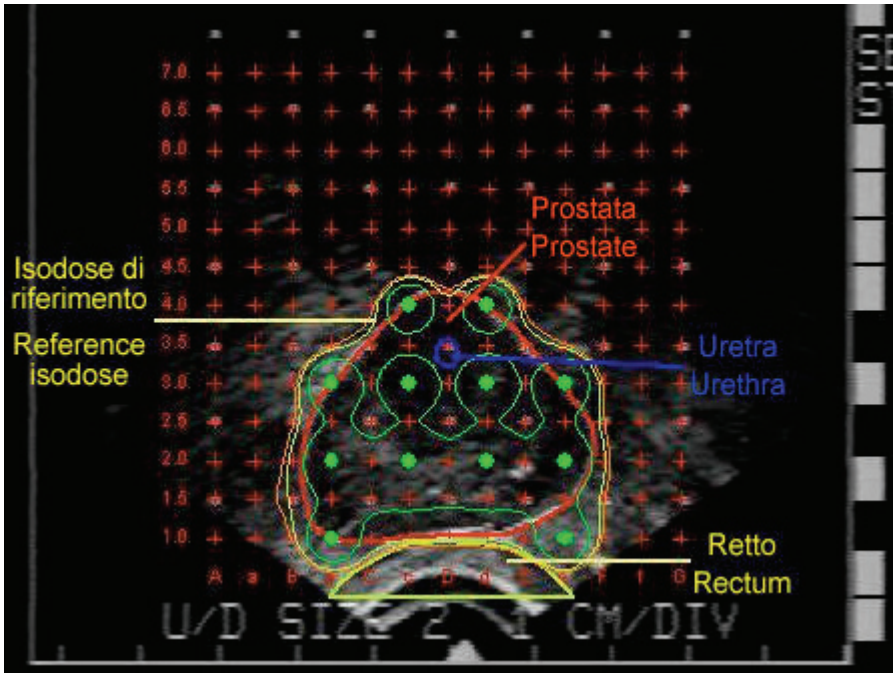


Figure 1.2 : Isodoses for a permanent brachytherapy treatment, showed on a US image of a prostate[7].

In the 1940's, Dr William G. Myers suggested to replace the impractical, expensive and uneasily available $^{226}Ra$ by $^{60}Co$. He later introduced or recommended the use of other radionuclides like $^{198}Au$ and $^{125}I$[8].

In 1972, permanent implantation of $^{125}I$ seeds in the prostate through surgical intervention was performed by Whitmore and Hilaris[5] but an accurate quality assessment for this technique was not possible with the technology of the time, causing variability in the results due to frequent inhomogeneity in dose distribution.

In 1983, Holms implanted seeds non-surgically, transpineally, using ultrasound for guidance[5] improving the accuracy and reproducibility of source placement. The technique was developed afterward by Radge and Blasko[5] who also devised a treatment planning method. It is also during the 1980's that a remote afterloading machine was commercialised for HDR.

Hence during the last 30 years, brachytherapy had an important development, partially due to the amelioration of imaging and remote afterloading techniques but also to the improvement of permanent treatment.

### 1.3. Classification of brachytherapy treatments

Brachytherapy treatments can be classified in function of dose rate at the prescription point. Low dose rate (LDR) treatment give dose at a dose rate of 2 Gy/h or less while high dose rate (HDR) treatment give dose at a dose rate higher than 12 Gy/h. A dose rate in-between could be classified medium dose rate (MDR), but that kind of treatment is not commonly used, mainly because of the poor results obtained in the few instances it's been tried[9].

Apart from the dose-rate limits defining LDR and HDR, the definition of those types of treatment has a practical interest, since the techniques used in both case are very different. HDR brachytherapy is given in a certain amount of fractions. Hence the implantation is always temporary. LDR brachytherapy is given in a continuous mode, i.e. the sources are left in the patient for all the duration of treatment, or in a very few numbers of fractions. LDR brachytherapy can be temporary (the sources is left for a certain period, and then removed) or permanent (the source is left inside the patient permanently).

### 1.4. Radionuclides used in brachytherapy treatment

Nowadays, brachytherapy is made mainly with $^{125}I$, $^{103}Pd$ for LDR treatments and $^{192}Ir$ for HDR treatments. Historically, other radionuclides like $^{226}Ra$, $^{60}Co$, $^{137}Cs$ and $^{198}Au$ have also been used. $^{226}Ra$ was the first radionuclide to be used for brachytherapy, but it decays to radon, which is a gas. This causes pressure in the capsule, making the use of that radionuclide in a closed source unsafe. So, for security reasons, radium is not used for brachytherapy anymore.

### 1.5. Types of brachytherapy implants

There are different types of brachytherapy implants, depending on the position of the implant. Those implants are intracavitary implants, interstitial implants, surface (mold) implants, intraluminal implants, and intravascular implants.

### 1.6. Medical context

The main (and more traditional) use of LDR permanent brachytherapy is the treatment of prostate. According to the website of the *Ministère de la Santé et des Services Sociaux du Québec*[10], in Quebec in 2002, there were 3548 new declared cases of prostate cancers (19.6 % of all new declared cancers), close second to lung cancer (20.8 % off all new declared cancers).

Permanent brachytherapy treatment is an outpatient procedure and permits a fast return to normal activities, with less complication than other treatments. It is proposed as an alternative to prostatectomy or other treatments to patient with early-stage localised prostate adenocarcinoma (it is necessary for the tumor to be localised since the seeds must be placed inside the tumor). It can't be performed for a patient with a prostate too small (less than 20cc)[7]. A prostate too large (more than 60cc) has to be reduced with hormonotherapy[7]. Permanent brachytherapy would also not be suggested to a patient who is suffering of severe urinary obstruction[7]. It can be performed alone or in conjunction with an external therapy treatment.

### 1.7. Recommendations and guidelines for permanent brachytherapy of prostate

Recommendations for permanent brachytherapy of the prostate were published by the American Brachytherapy Society (ABS)[11,12,13]. Guidelines for permanent brachytherapy of prostate were given in TG-64[14]. The ABS and theTG-64 recommends that two distributions of dose are studied for each treatment. The *pre-implant* plan is made before the implantation, assuming an ideal distribution of the seeds. This pre-implant plan constitutes the actual treatment planning and it is at that point of the treatment that optimisation is made. The *post-implant* plan, more representative of reality, is made after the implantation to check the quality of the implant, study the treatment outcome and compare different cases.

#### 1.7.1. DVH

Dose volume histograms (DVH) for the *planning target volume* (PTV) and other organs are used to study and to compare implants. Parameters such as the

$D_{90}$, $D_{80}$, $D_{50}$, $D_{10}$, $V_{100}$ and $V_{200}$ are used to study the plan outcome and to compare one plan to another. In that notation, $D_X$ correspond to the dose given to at least X % of the target while $V_X$ correspond to the volume that receives at least X % of the prescribed dose. A DVH is illustrated on figure 1.3 .

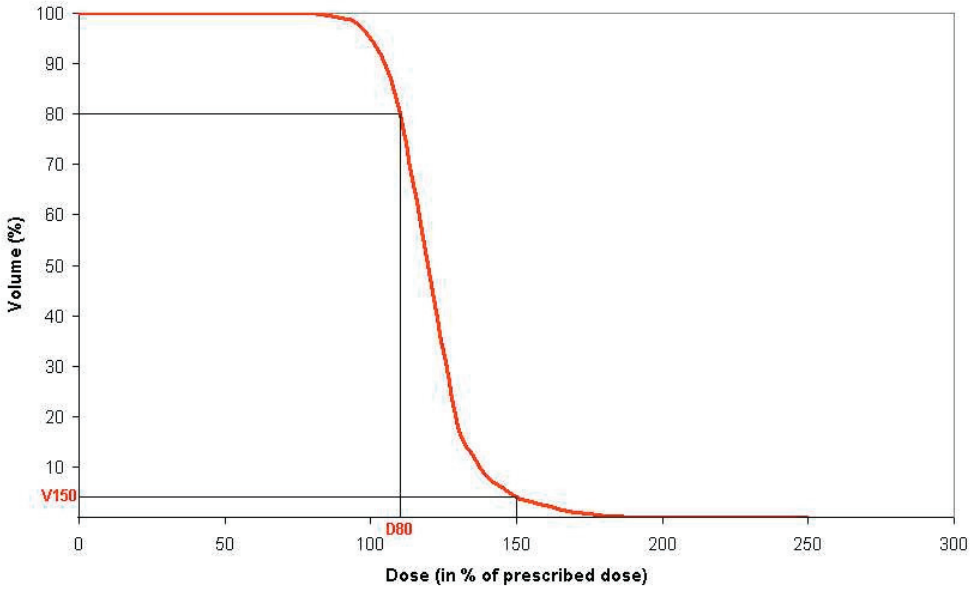


Figure 1.3 : Schema of a DVH. The D80 (dose given to 80% of the volume) and V150 (volume receiving 150% of the prescribed dose) are indicated in red.

### 1.7.2. Prescription

When permanent brachytherapy is used alone, the prescribed dose for the implant should be 144 Gy for $^{125}$I implants[1,14] and 115 Gy to 120 Gy for $^{103}$Pd implants[11]. This is the dose that should cover the PTV in the pre-implant plan (V100 should be equal or close to the prescription dose).

In TG-64[14] the *minimum peripheral dose* (mPD) is defined as the isodose surface that encompasses the PTV. Ideally, giving the prescribed dose to the mPD in the pre-implant plan would ensure giving it to all the target volume ($D_{100}$ from post implant geometry would be 144 Gy). However, because of diverse factors (seed placement errors, migration of seeds, organs oedema and movement, etc.) the dose distribution might be different than what could be expected by simply looking at the pre-implant plan and TG-64 recognises that the dose given to all the PTV might

actually be different from 144 Gy. Other ways to report prescription are mentioned in TG-64, but it is stated that the other methods doesn't provide as good information about coverage.

If the mPD is mentioned in the ABS recommendations[11] as having been used for prescription in certain cases, other parameters are also considered like $D_{90}$ for the prostate, $D_{30}$ for the urethra and the volume of rectum getting the prescription dose[13]. An effort should also be made to minimise the length of urethra getting more than 200% of the prescribed dose[11].

### 1.7.3. Pre-implant plan

A pre-implant plan is made before the seeds implantation, in order to get the best coverage of the target while limiting dose to the surrounding organs, controlling dose inhomogeneity and keeping the implant as simple as possible. Even if this pre-implant gives good indications, it is important to keep in mind that many factors will have an influence during and after implantation so that the actual implant will be different from this pre-implant[11,14].

Note that an intraoperative plan can also be made, based on TRUS imaging, just before implantation[11,13,14]. This will optimise the treatment by taking into account the position of the prostate that might have moved or changed volume since the first image was taken. The optimised seed positioning is made just before the implantation. Ideally, such an intraoperative planning should be used[11].

First, an image-based volume study is made[14]. The ABS recommends the use of TRUS but the use of CT or MRI is also reported[11]. The images used for this purpose need to be taken no more than 2-3 weeks before the implantation and consists of axial slices at least 5 mm thick[14]. For the case of an intraoperative planning, the images taken in advance (not including the images taken in the treatment room for treatment planning) can be limited to the determination of the pubic arch interference and to a volumetric measurement to select the source strength[14].

The planning must take into account the pubic arch interference that might make it impossible to put seeds in some portions of the prostate. This can

sometimes be corrected by inclining the template during implantation but that correction is limited. Pubic arch interference could even be a contraindication for permanent implant in some extreme cases. The position of urethra and rectum anterior wall is also taken into account in the planning, since high doses to those organs are known to increase the risk of complications.[14]

A hole pattern of the template for the needles that will be used for implantation is superposed on the image to plan the seeds position. TG-64[14] describes three different ways to make the seed distribution. The simpler, *uniform loading*, consists in putting the seeds 1 cm apart uniformly in the prostate. This method gives a large dose at the center of the prostate, including the prostatic urethra. In *modified peripheral loading*, some seeds at the center of the uniform distribution are taken out and the strength of the other seeds is increased or they are placed closer to compensate. *Peripheral loading* gives a minimum dose (but still higher than the prescribed dose) to the urethra by limiting the seeds to the periphery, while increasing their strength. The two last methods are more used today since they limit the overdose to the urethra. Apart from the three methods described in TG-64, diverse commercial systems now include the possibility to use inverse planning[13] which permits to optimise the seed distribution and obtain quality plans in a timely fashion. Inverse planning is very useful for intraoperative planning.

### 1.7.4. Post-implant study

Because of seed placement errors, oedema of the prostate and motion of seeds and organs, the implantation result is never exactly as planned and a post-implant dosimetric evaluation is necessary[11,12,14]. A waiting period of about 28 days between implantation and imaging is recommended[12,14], so that oedema has time to resolve. Then, it must not be forgotten that the total dose determined in the post-implant study might be overestimated, because during that oedema period the seeds are more distant which is not considered in the determination of the total dose distribution[14]. However, for practical reasons, a shorter waiting time might be chosen. Then, the waiting period should be consistent in each center[12].

For the post implant study, films, MRI or TRUS can be used, but the use of CT with contiguous axial slices no larger than 5 mm is recommended by the ABS[12].

In each CT slice, the prostate is outlined and each seed is localised. The dose is calculated to each point of a 3D matrix. Isodose curves are superposed to each of the CT slices and a DVH is generated for the PTV. DVH for other organs like urethra and rectum can also be made for a more complete study. Hence, qualitative and quantitative study of the target coverage, dose uniformity and dose conformity can be made using the isodose distribution and the $D_X$ and $V_X$ parameters from the DVH[11,14].

### 1.8. Thesis overview

In the present work, two effects in permanent LDR brachytherapy will be studied. The first effect is the perturbation due to the presence of the seeds (*interseed effect*). The second effect is the impact of the tissue composition (*tissue-composition effect*).

In chapter 2 a review of the TG-43 protocol, used for brachytherapy dosimetry will be made and the limits of the dosimetry made using this protocol will be presented. In chapter 3, we will discuss the tools that were used to do our study. Monte-Carlo (MC) simulations were made to study the impact of the two effects on dosimetry. In order to validate our simulations, measurements were made with TLDs and with Gafchromic® EBT films (after that detector was validated to determine dose around LDR brachytherapy sources). In chapter 4, we will discuss the results of our simulations and measurements. Finally, in chapter 5, we will present a brief conclusion and discuss of future work that could be done to develop and continue the study.

# Chapter 2. The TG-43 protocol

## 2.1. General description of the TG-43 protocol

LDR brachytherapy dosimetry is generally made using the TG-43 protocol[15] and its update, TG-43U1[16]. In this protocol, the dose rate is determined at each point around one seed, in homogenous water. The dose rate distributions of individual seeds are superposed to determine the dose rate distribution for the whole implant.

TG-43 dosimetry is made using different parameters. In order to make the dosimetry uniform between different centers, *consensus data* for those parameters are tabulated based on different studies. It is recommended that the parameters for a new model be published before using it clinically. A supplement to the update of TG-43 (TG-43U1S1) was published in June 2007[17] determining consensus data for diverse seeds models that went out after the publication of TG43U1, including IBt interseed[125] model (hereafter referred to as IBt). For the IBt model the data in TG-43U1S1 was determined using the results published by Reniers *et al.*[18], based on work detailed in reference 19, and Meigooni *et al*[20]*.*

Figure 2.1 shows the coordinate system used in TG-43. Note that the plane perpendicular to the seed and cutting it in the middle of the radioactive area (xy plane on the figure) is called the *transverse plane* while the axis along the seed and in its middle (z-axis on the figure) is called the *longitudinal axis*.

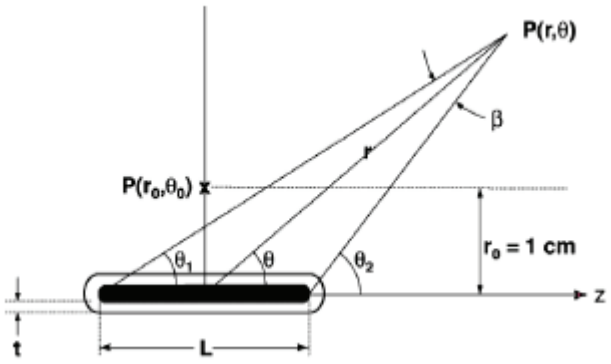


Figure 2.1 : Coordinate system for TG-43 dosimetry[15].

## 2.2. TG-43 parameters

Dosimetry using TG-43 can be based either on a line source approximation or on a point source approximation. In the next notation, the subscript *L* stands for the line source approximation, the subscript *P* stands for the point source approximation and the subscript *X* stands for either *P* or *L*. Apart for the Air-kerma strength, the parameters are defined in water.

$S_k$ is the *air-kerma strength*, indicating the strength of the source. The unit of *Sk* is U, with 1 U = 1 μGym$^2$h$^{-1}$ = 1 cGycm$^2$h$^{-1}$.

$$S_k = \dot{K}_\partial(d)d^2 \tag{2.1}$$

In that equation, $\dot{K}_\partial(d)$ is the air-kerma rate due to photons of energy superior to a cut-off δ. It is defined *in vacuo* and normally measured in air, and corrected for attenuation. The cut-off energy (typically 5 keV) is used to eliminate the contamination of characteristics photons created in the outer layers of the source. The distance from the seed, d should be large enough for the seed to appear as a point source.

Λ is the *dose rate constant*, in units of cGyU$^{-1}$h$^{-1}$. It gives the dose rate to water, per unit of $S_k$ at a point of reference defined at $r_0$ = 1 cm and θ = 90° (in the transverse plane of the seed).

$$\Lambda = \dot{D}(r_0,\theta_0)/S_k \tag{2.2}$$

The *geometry function*, $G_X(r,\theta)$, takes into account the inverse square law and the spatial distribution of the activity in the seed.

$$G_X(r,\theta) = \begin{cases} r^{-2} \rightarrow point-source \\ \beta / Lr\sin\theta \rightarrow line-source, \theta \neq 0^o \\ 1/\left(r^2 - L^2/4\right) \rightarrow line-source, \theta = 0^o \end{cases} \tag{2.3}$$

The *radial dose function*, $g_X(r)$ takes into account the absorption and scattering along the transverse axis.

$$g_X(r) = \dot{D}(r,\theta_0)G_X(r_0,\theta_0)/\dot{D}(r_0,\theta_0)G_X(r,\theta_0) \tag{2.4}$$

The *anisotropy function* takes into account the anisotropy around the seed. The 2D anisotropy function is noted $F(r,\theta)$.

$$F(r,\theta) = \dot{D}(r,\theta)G_L(r,\theta_0)/\dot{D}(r,\theta_0)G_L(r,\theta) \tag{2.5}$$

The 1D anisotropy function is noted $\phi_{an}(r)$.

$$\phi_{an}(r) = \frac{\int_0^{\pi} \dot{D}(r,\theta)\sin\theta d\theta}{2\dot{D}(r,\theta_0)} \tag{2.6}$$

### 2.3. 2D and 1D protocols

The TG-43 2D protocol is based on a line-source approximation. The general formula for the 2D protocol is given in equation 2.7.

$$\dot{D}(r,\theta) = S_k \Lambda[G_L(r,\theta)/G_L(r_0,\theta_0)]g_L(r)F(r,\theta) \tag{2.7}$$

TG-43 also proposes a 1D protocol that can be based on a point-source approximation or on a line source approximation, with the general formula shown in equation 2.8.

$$\dot{D}(r) = S_k \Lambda[G_X(r,\theta_0)/G_X(r_0,\theta_0)]g_X(r)\phi_{an}(r) \tag{2.8}$$

Note that for the point source approximation the term in brackets can be reduced to $(r_0/r)^2$.

### 2.4. Advantages of the TG-43 protocol for treatment planning

The TG-43 protocol is very useful for brachytherapy treatment planning. The dosimetry is made with calculations based on tabulated values. In addition to the fact that the use of tabulated values permits to standardise the dosimetry between centers, the calculations can be made with a treatment planning system at an acceptable speed (less than a second). The advantage of obtaining a plan quickly is not negligible, since it permits to make the optimisation just before the treatment.

### 2.5. Problems with TG-43

TG-43 is a very useful tool for LDR brachytherapy treatment planning, but one might discuss the accuracy of dosimetry based on the TG-43 protocol. TG-43 is

based on certain approximations that can have a significant impact on the dose distribution and the treatment outcome.

### 2.5.1. Interseed effect

The first assumption is that the total dose distribution for a multi-seed implant is merely the superposition of the dose distributions due to each seed independently. This assumption implies that the seeds themselves don't have a significant impact on the dose. However, each seed perturbs the distribution due to its neighbours, causing an interseed effect.

*Interseed effect* was defined in 1992 by Meigooni *et al*.[21] as the ratio of the dose to a point due to an implant as a whole over the sum of the individual doses due to all the seeds in the implant, for a multi-seed implant configuration. More generally, the *interseed effect* or *interseed attenuation* is the impact of the seed attenuation on the dose distribution, DVH and even treatment outcome.

$$Interseed\ \ effect = \frac{\dot{D}_{1+2+3}}{\dot{D}_1 + \dot{D}_2 + \dot{D}_3} \tag{2.9}$$

This effect was first studied by Burns and Raeside[22] in 1989, although they did not called it the *interseed effects*, being more interested in the attenuation due to each seed. They defined a *perturbation factor* as the ratio of the dose to a point due to an active seed with and without inactive neighbours.

$$Perturbation\ \ factor = \frac{\dot{D}_{with\ neighbours}}{\dot{D}_{without\ neighbours}}\left(for\ one\ active\ seed\right) \tag{2.10}$$

Burns and Raeside[22] made an MC study for 2 and 4 coplanar seeds, with only one source active, for two different seed models (6711 and 6072). They made interesting observations. The perturbation factor depends on the model of the seed. There is more perturbation for model 6711, which contains a silver wire, than for 6702, which contains three resin spheres. The perturbation affects mainly the primary radiation. Hence the factor goes toward one as we go farther from the active seed for a fixed spacing (since the proportion of primary diminishes) and toward a lower limit at a fixed distance from the seeds for model 6711 as the seeds go closer together (the silver wire in 6711 absorbs almost all the primary, explaining the limit).

There is no significant perturbation in between the seeds (no backscatter from the second seed) and outside of the geometrical shadow of the neighbouring seed (no change in scatter from the primary).

Meigooni *et al.*[21] made measurements with TLDs for three seeds of the same models studied by Burns and Raeside, parallel or co-aligned. They measured the dose rate for the seeds individually and all together. For parallel seeds, the sum of individual doses is about 8 % higher than the dose measured for all seeds together. However, they observed no significant interseed effect when the seeds are longitudinally aligned. This could be explained by the fact that the dose in the longitudinal prolongation of the seed is mainly due to scatter, which is not affected by the other seeds.

Both teams have studied the error on dose due to the presence of other seeds, for an implant. Burns and Raeside[22] calculated the difference between the dose uncorrected and corrected using the perturbation factors, for one plane and two planes of 16 seeds. They observed that the error is higher for 6711 and when the seeds are closer, which is not a surprise since the perturbation is more important for both those cases. The error is smaller for the two-plane than for the one-plane implant because a smaller proportion of seeds is shadowed for the two-plane implant. The maximal error occurs inside the seed array (up to 10 %) but the corrected doses are higher than the prescribed dose (defined in periphery) so the inside of the implant is not underdosed. However, the perturbation effect might be significant in the periphery of the implant, where the given dose would be lower than the prescribed dose.

Meigooni *et al.*[21] compared the measured dose with the result of a treatment planning system, for two planes of 9 seeds. The average error in periphery of the implant for $^{125}$I seeds is 6 %. They concluded that this effect is significant and should be taken into account for treatment planning, a conclusion discussed in TG-64[14] :

> While the dosimetric impact of the interseed effect may be of clinical concern in simple, regular configurations, the overall effect in prostate implant is not clear. In practice, only the nearest-neighbour seeds are likely to produce appreciable dose perturbation. The solid angle sustained by a seed at 1 cm average distance is sufficiently small that the volume of perturbation is for most purpose negligible.

More recently, work has been done to determine the effect of diverse factors on clinical plans. In 2005, Chibani et al.[23] studied the effects of anisotropy and interseed attenuation by comparing 3 models, for idealised and clinical prostate implants, for $^{125}$I (IsoSeed) and $^{103}$Pd (Theraseed 200). The first model is a point source dose kernel superposition (PSKS) which is isotropic and based on the 1D formalism of the TG-43U1 protocol. The second is a line source dose kernel superposition that is anisotropic and based on the 2D formalism. The third is a full MC simulation (FMCS) which takes into account the anisotropy and interseed effect. The interseed effect is illustrated by the difference between the LSKS and the more accurate FMCS. In most cases, the LSKS overestimate the dose received by the patient. For $^{125}$I the results of LSKS are higher than those of the FMCS by an average of 3-4 %. The prostate DVH is right-shifted if we neglect the interseed effect, so that the volume receiving more than $D_{90}$ is overestimated (3-3.5 % for 1.5 x $D_{90}$ and 7-10 % for 2 x $D_{90}$ for an ideal implant). $D_{80}$, $D_{90}$ and $D_{100}$ are systematically overestimated. This is less evident for the DVH for the urethra, rectum and margin around the prostate.

Mobit and Badragan[24] calculated using MC (EGSnrc) the distributions obtained by superposing the dose distribution for one seed and by simulating all the seeds in a 27-seeds plan. The seeds, model 6711 were uniformly distributed in three planes of nine seeds. The comparison was made for separations of 0.5 cm, 0.75 cm and 1 cm separations. In all cases, the superposition of the single seed distribution overestimate the dose by up to 10%, but the region occupied by the large difference gets bigger as the spacing between the seeds diminishes. Even though local differences are observed for all seed spacing, the difference in DVH is significant only for the 0.5 cm for which the DVH is right-shifted for the single seed superposition compared to the simulation for the whole implant. Also, for the 0.5 cm separation, the single seed superposition would overestimate the dose inhomogeneity inside the implant and the dose given outside of the target (hence it could overestimate the dose to OAR). However, it would also overestimate the coverage of the target. For the 1 cm separation, the difference in coverage, dose homogeneity and dose given outside of the target would not be clinically significant.

Since in clinical implants the separation is usually 1 cm, Mobit and Badragan[24] conclude that the use of the single seed superposition would not have a significant clinical impact, but no attempt is made in that particular study to evaluate the effect of seed migration that might bring some seeds closer to each other.

In their study of the effects of interseed attenuation and tissue composition, Carrier *et al.*[25,26] studied realistic implants. The first study[25] was made for pre-implant plans for different seed densities, in two sizes of prostate. The second study[26] was made for post implants seed distributions determined with CT images of 28 real implants, seed model selectSeed (with a geometry similar to model 6711). Four different calculation techniques were compared. The first one is a TG-43 based calculation (corresponding to the LSKS from Chibani *et al.*[23]) and is used to validate the second one, the superposition of MC (Geant4) distribution for one seed (SMC in reference 25 and NoSeedMC in reference 26). After verification of its correspondence with the line source TG-43 calculation, the SMC, representing the TG-43 results, is used for comparison with the following models. The third model is the full MC with water prostate (MCW in reference 25 and WaterMC in reference 26 - corresponding to the FMCS from Chibani *et al.*[23]) which takes the interseed effect into account. The fourth, the full MC with realistic prostate tissues (MCP in reerence 25 and CompleteMC in reference 26), takes the interseed effect and the prostate composition into account. The comparison between SMC and MCW indicates how neglecting the interseed effect affects the treatment planning. In all cases, the SMC overestimates the studied parameters ($D_{90}$, $D_{50}$, $D_{10}$, $V_{100}$ and $V_{200}$)[25]. Normally, the interseed attenuation augments with the seed density (which is expected since there is more perturbation when the seeds are closer), but characteristics of a particular plan can have an impact[25]. The average overestimation on the post implant studies due to ignoring the interseed effect would be 4.2% on $D_{90}$ and 1.2% on $V_{100}$, with large variations from one case to another[26].

### 2.5.2. Tissue composition effect

The second assumption is that the seeds are in an infinite volume of water, while in reality, they are in a patient who is a finite volume composed of

heterogeneous tissues. The absence of tissue outside the patient influences the distribution because of the absence of backscatter. It has been showed that, for full scatter conditions to be obtained (i.e. for the dose distribution to be similar to the dose distribution in an infinite phantom), tissue must extend 5 cm farther than the most distal point of interest[16,27]. For instance, a 15 cm radius sphere is recommended to determine the TG-43 parameters up to 10 cm from a seed. This means that in order to get full scatter condition in an actual patient, the limits of the region of interest (including the OARs) needs to be at least 5 cm inside the limits of the patient. If this full scatter condition will be obtained in prostate treatment will depend on the position of the ROI compared to the skin and will depend on the case, but can clearly have an impact, particularly for breast implants.

The different composition in respect to water have an impact because of the tissue composition effect. At low energy, the photoelectric effect is more important or dominant. For instance, in water for 30 keV photons, the cross-section for photo-electric effect is 39% of the total cross-section for all interactions, compared to 0.005% for 1 MeV photons[28]. Because of the importance of photoelectric effect at LDR brachytherapy energies, the tissues are not all water equivalent and the material can have a significant impact on dose distribution and treatment parameters.

The impact of material composition for $^{125}$I source dosimetry was studied by Meigooni et al.[29] in 1988, but at that time, the goal of the study was to determine which solid phantom material was water equivalent. They measured with TLDs and calculated with MC the dose rate at different distances from a seed in Solid Water, Polystyrene and PMMA and compared the results with MC calculation results, in water. They determined that at $^{125}$I energies, the Solid Water is water equivalent, but not the polystyrene and the PMMA.

The comparison between the MCW and MCP of Carrier *et al.*[25,26] indicates how the water estimation affects the treatment planning. From their pre-implant study[25], they observed that the difference is independent of the number of seeds[25]. The water estimation doesn't affect the volume coverage ($V_{100}$). However, the MCW overestimate other parameters. For example, the MCP gives a result that is 3.6 %

smaller than the MCW for the $D_{90}$. This difference is due to the change in elemental composition (2.5 %) and density (1.1 %). This was determined by simulating the seed in a tissue of prostate composition and water density. For the post implant study[26] of real implants, ignoring the tissue composition effect would cause an overestimation of 2.6% in $D_{90}$ and 0.9% on $V_{100}$ with very small variation from one case to another. The dose to organs at risk (OAR) is also overestimated by ignoring both effect[26].

Hence, both the interseed effect and the tissue-composition effect diminish the different parameter so that the treatment planning based on TG-43 overestimate the dose given to patient. The total effect was also studied by Carrier *et al.* The overall comparison between the TG-43U1 based calculation and the more realistic MCP indicates the accuracy of the treatment planning. In the pre-implant plans[25], the dose calculated with TG-43U1 is overestimated by 3.4 to 8.2 %. The $D_{90}$ is overestimated by 1.2 % to 8 %. For the post implant study[26], the average total overestimation would be of 6.8% on $D_{90}$ and 2.3% on $V_{100}$. Consequently, the delivered doses are smaller than expected when calculated using the TG-43 formalism.

### 2.5.3. Proposed solution : MC planning

Many assumptions are made in the TG-43 protocol and it would be interesting for the dosimetry to be closer to reality. This could be achieved by doing the dosimetry with MC. This dosimetry would give a better knowledge of the actual dose distribution. That better knowledge might have an impact on the understanding on the treatment outcome. However there are some problems with such a dosimetry. The principal problem is that the time necessary to obtain the distribution is very long (a few hours to a few days) compared to planning based on TG-43. Hence, such a method is still impractical without further improvement on speed, particularly for the optimisation before the treatment.

Because of the long calculation times implied for MC calculations, pre-treatment optimisation is not practical with this method. However, it might be argued that for the post-implant study, speed is not the main issue and a better knowledge

of the actual dose distribution given to the patient would be useful, particularly for long-term studies of the treatment outcome. Hence planning and optimising with TG-43 before the implantation while doing the post-implant study with MC could be an interesting option.

Some teams like Carrier *et al.*[26] are working on the use of MC to do the dosimetry for the post-implant study. The goal of their study is to obtain a dosimetry in a realistic patient. The seeds are all simulated in order to take the interseed effect into account. To consider the tissue-composition effect and the absence of backscatter, the patient is reproduced as precisely as possible by separating the model into voxels that are filled with the accurate material, based on the CT image made after the implantation.

# Chapter 3. Material and method

## 3.1. MC simulations

### 3.1.1. General

MC methods are used to simulate virtual systems that are as close as possible to the reality they represent. These methods use statistics to calculate the effect of a phenomenon (radiation in the case that interests us). Each element of the phenomenon (transport and interactions of each particle in the case of radiation) is simulated and the behaviour of the physical system is inferred from the behaviour of the simulated system.[30] In medical physics, MC methods are used to simulate the reality with accuracy by solving the equation of transport, in order to determine values such as the deposited energy or the particle fluence.

To simulate the effects of radiation, particles are created in a source and transported in a medium. Diverse interactions occur during each particle transport. Due to those interactions, the particle is absorbed or scattered and other particles are created and will eventually be transported. The type of interaction and the type, energy and direction of the produced particles are determined randomly using the cross-sections of the diverse interactions. That way, if a sufficient number of particles is used in the calculation, the result of the simulation will be representative of the reality.

### 3.1.2. Code MCNP4C

For this work, the MC simulations were performed using code MCNP4C[30]. This code is very user-friendly and permits an accurate representation of the desired geometry. In the input file, geometrical volumes called cells are delimited by surfaces and filled with the desired material. The material is defined with its elemental composition and density. The source definition is made by selecting the geometric distribution from where the radiation is coming and the spectrum of emission of such radiation. For LDR brachytherapy, this consists in giving the distribution of the

radionuclide in the seed and in saying in which proportions the energy of the emitted photons is distributed.

#### 3.1.2.1. Detailed physics treatment

The code MCNP4C allows the use of simple or detailed physics treatment[30]. The detailed physics treatment takes into account every type of interaction with a good simulation of their products while the simple physics treatment approximates or ignores some of the interactions. In LDR brachytherapy, we need to use the detailed treatment, in order to account for photoelectric effect with emission of fluorescent photons, Rayleigh (coherent) scattering and Compton effect (incoherent scattering), with Doppler broadening and binding effects.

#### 3.1.2.2. Tallies

Different quantities of interest can be tallied, or counted, using MC. The MCNP code offers seven different tally types with different possibilities of modification. All are expressed per source particle. Three tallies were used in this work. The definition for each tally is given in the MCNP4C user manual[30].

The *track length estimate of cell flux* (tally F4), is defined as the quantity :

$$F_4 = W * \frac{T_1}{V} \tag{3.1}$$

it estimates :

$$F_4 = \int_V \int_t \int_E \Phi(\vec{r}, E, t) dE dt \frac{dV}{V} \tag{3.2}$$

with :

$W = particle\ weight$

$T_l = track\ lenght\,(cm)$

$E = particle\ energy\,(MeV)$

$V = volume(cm^3)$

$\Phi(\vec{r}, E, t) = particle\ flux$

The definition of the particle flux is $\Phi(\vec{r}, E, t) = vN(\vec{r}, E, t)$, the product of the particle velocity and the particle density.

F4 is expressed in $cm^{-2}$. Note that the tally can be multiplied by the energy with the notation *F4 to give the energy fluence :

$$*F_4 = \int_V \int_t \int_E E * \Phi(\vec{r}, E, t) dE dt \frac{dV}{V} \tag{3.3}$$

The *energy deposition averaged over a cell* (F6), is defined as :

$$F_6 = W * T_1 * \sigma_T(E) * (E) * \frac{\rho_a}{m} \tag{3.4}$$

It gives an estimate of :

$$F_6 = \frac{\rho_a}{\rho_g} \int_V \int_t \int_E H(E) \Phi(\vec{r}, E, t) dE dt \frac{dV}{V} \tag{3.5}$$

with :

$W = particle\ weight$
$T_l = track\ lenght(cm)$
$\rho_a = atomic\ density(atom/barn - cm)$
$\rho_g = gram\ density(g/cm^3)$
$E = particle\ energy(MeV)$
$m = cell\ mass(g)$
$V = volume(cm^3)$
$\Phi(\vec{r}, E, t) = particle\ flux$
$H(E) = Heating\ number$

For photons F6, the heating number is defined as :

$$H(E) = \sigma_T(E) \sum_{i=1}^{3} p_i(E) * (E - \overline{E}_{out}) \tag{3.6}$$

where $\sigma_T(E)$ is the total cross section, $p_i(E)$ is the probability of reaction *i* (1 = Compton scattering, 2 = pair production, 3 = photoelectric effect), $E$ is the incident energy and $\overline{E}_{out}$ is the average exiting energy.

F6, expressed in MeV/g gives the KERMA (kinetic energy released in media) in the desired cell. Note that F6 is not offered for electrons. Also, F6 is a special case of F4 with an energy-dependant multiplier.

The *pulse height tally* (tally F8), expressed in pulses gives the energy distribution of pulses created in a cell.

$$F_8 = W_s \; put\, in\, bin\, E * \frac{W}{Ws} \tag{3.7}$$

with $W = particle\ weight$ and $W_s = source\ weight$ .

This tally multiplied by the energy (*F8) is expressed in MeV and gives the energy deposited in a cell. Divided by the cell mass, this gives the dose in the cell.

Contrary to the F4 and F6 tallies that give an estimate of energy deposited based on track length, tally F8 is analogous to an actual detector in the sense that it counts the energy deposited by each particle during an interaction in the cell. If this is interesting in some case, that tally is also time consuming and does not permit a lot of variance reduction techniques.

In many applications, for low energy emitters like $^{125}$I, the electron transport can be cut, so that the electrons are assumed to deposit their energy on the spot of their creation. This is justifiable because the range of the electrons is much smaller than the sampling region. In this case, the dose in a cell can be approximated by the kerma and tally F6 can be used. This is very efficient and permits to obtain good statistics with relatively small calculation time compared to the *F8 tally. That assumption was used for many of our simulations. In cases where the dose to water in a different media is computed, the more general tally F4 modified with a multiplicator was used.

### 3.1.3. Seed simulation

#### 3.1.3.1. Geometry

The seed studied in this work is IBt™ Interseed-125 (IBt). This seed consists of two concentric titanium cylinders welded at the extremities. A platinum ring marker is covering the center of the internal cylinder. A $^{125}$I radioactive paint is applied around the internal cylinder and the platinum marker. A schema of the seed is presented on figure 3.1 . MCNP4C was used to simulate the seed as accurately as possible. Our simulation of the seed is represented on figure 3.2. Of course, the welding between the titanium cylinders has to be approximated. In our simulations, cones approximated the welding, as it was for the simulations of Reniers[19].

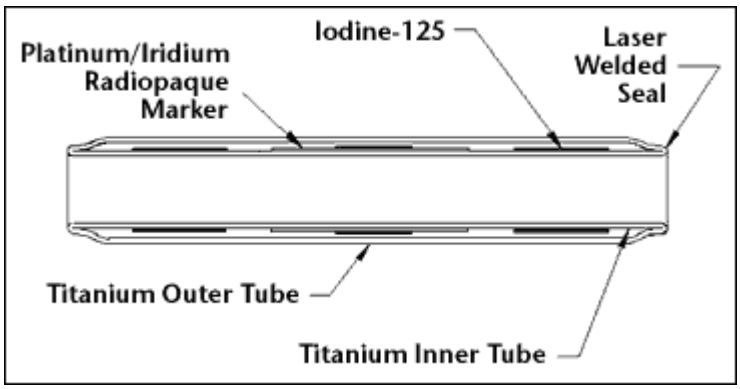


Figure 3.1 : IBt Interseed-125 seed[31].

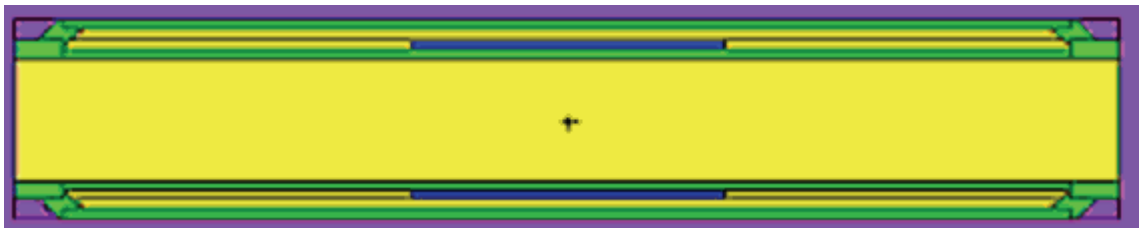

Figure 3.2 : Simulation of IBt Interseed[125] seed. Purple : water, green : titanium, blue : platinum, yellow :air.

Note that in our simulations the interior cylinder of the seed is filled with air. It could be assumed that in the patient, the hollow cylinder might get filled with fluids and tissues. The impact of that is not studied in the present work. It was mentioned by Reniers[19] in a private communication that this didn't had a significant impact on the dose distribution around the seeds and on the TG-43 parameters.

The simulations were made using MCNP4C. The detailed physics treatment was used. In most of our simulation, there was no transport of electrons and tally F6 was used. Tally F4 with a multiplicator was used for simulations in tissue when the dose to water in a different material was needed.

#### 3.1.3.2. Validation

We simulated one seed in water in order to determine TG-43 parameters that will be used for the TG-43 calculations in our realistic implant study. To validate our simulations, our results were compared with those published by Reniers[19]. The scoring regions were limited by spherical shells of 1 mm thickness, placed every 0.5 cm, up to 7 cm from the seed. Cones were placed every 10° along the

longitudinal axis to subdivide the spheres. Along the transverse plane ($\theta$=0) planes with a 1 mm separation were used in place of the cones. This geometry is illustrated in figure 3.3. Comparatively, Reniers[19] only used cones. Our use of planes is justified by the fact that the same simulation were later used to compare the radial dose function in water with radial dose function in different materials, also calculated using planes. Tally F6 was used to determine the kerma every 10 degrees and every 0.5 cm. This gave us the kerma distribution around the seed, in coordinates of r and θ. In order to diminish the statistical uncertainty 20 000 000 particles were simulated. Reniers used the same tally and simulated 5 000 000 particles[19].

The geometry factor is calculated at each point (i.e. its value is independent of measurement or simulation results), using the linear approximation (equation 2.3). Calculated values for certain points are given in table 3.1.

The radial dose functions at diverse distances were calculated with equation 2.4 , using our simulation results for $\theta = 90^{o}$. Results are shown in table 3.2 and figure 3.4. The average difference with results obtained by Reniers[19] is 0.4 %, with a maximum difference of 2.7 % at 6.5 cm from the seed (a positive sign on the difference indicates that we overestimated the factor while a negative sign indicates that we underestimated the factor, compare to Reniers). The differences can be due to the MC statistics and to the shape of the scoring zones. For the maximal difference at 6.5 cm from the seed, the statistical uncertainty might be responsible of about 1.3% since the statistical uncertainty is 0.8% for both our simulation and Reniers's at that distance. At that same distance, a simulation made for another purpose showed a 3% difference between a scoring zone delimited by a cube and by the section of a cone. Hence, considering the statistical uncertainty and the difference in scoring zones, the differences with Reniers are acceptable. A fit on our results, was made using Excel and will be used in a Matlab program for TG-43 calculations (equation 3.8).

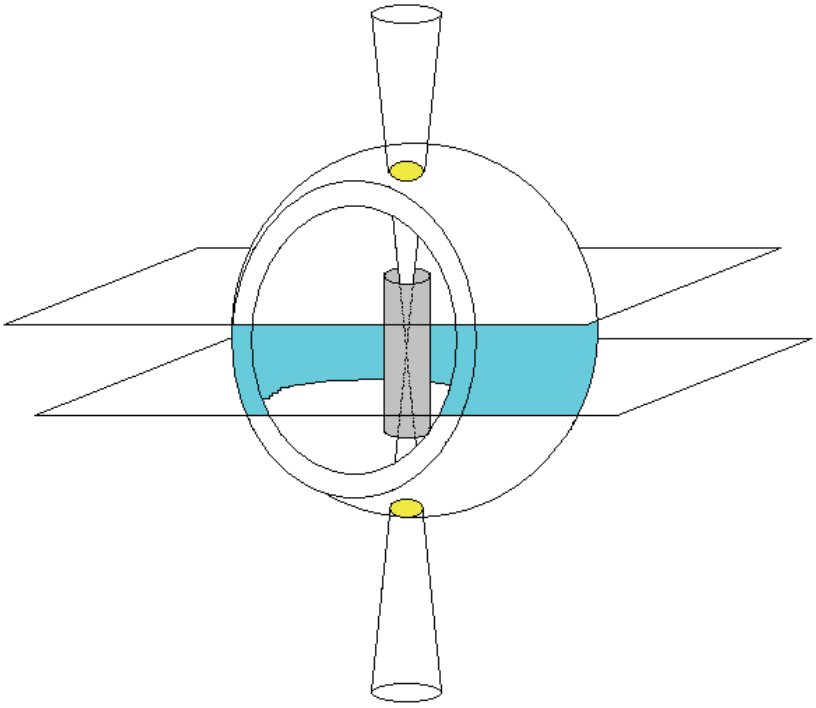

a)

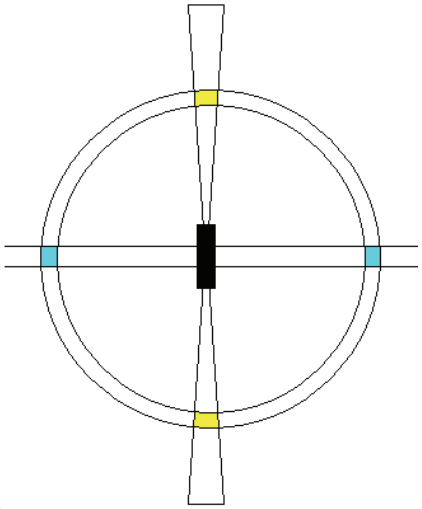

b)

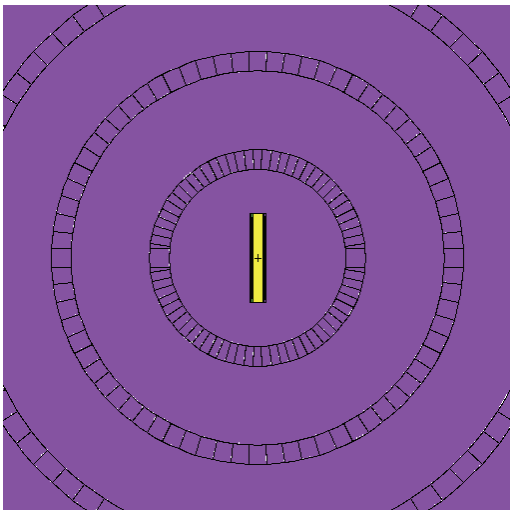

c)

Figure 3.3 : a and b) 3D (a) and 2D (b) schematisation of the geometry with only one sphere, one cone and the plane surfaces shown for simplification. The scoring region at $0^{o}$ is shown in yellow while the scoring region at $90^{o}$ is shown in blue.
c) distribution of the scoring zones around the seed.

Table 3.1 : G(r,θ) around IBt Interseed[125].

| r (cm) \ Θ | 0 | 10 | 20 | 30 | 40 | 50 | 60 | 70 | 80 | 90 |
|---|---|---|---|---|---|---|---|---|---|---|
| 0,5 | 4.634 | 4.601 | 4.508 | 4.378 | 4.236 | 4.101 | 3.986 | 3.901 | 3.849 | 3.831 |
| 1,0 | 1.035 | 1.034 | 1.030 | 1.023 | 1.015 | 1.007 | 1.000 | 0.994 | 0.990 | 0.989 |
| 1,5 | 0.451 | 0.451 | 0.450 | 0.449 | 0.447 | 0.446 | 0.444 | 0.443 | 0.442 | 0.442 |
| 2,0 | 0.252 | 0.252 | 0.252 | 0.251 | 0.251 | 0.250 | 0.250 | 0.250 | 0.249 | 0.249 |
| 2,5 | 0.161 | 0.161 | 0.161 | 0.161 | 0.160 | 0.160 | 0.160 | 0.160 | 0.160 | 0.160 |
| 3,0 | 0.112 | 0.112 | 0.111 | 0.111 | 0.111 | 0.111 | 0.111 | 0.111 | 0.111 | 0.111 |
| 3,5 | 0.082 | 0.082 | 0.082 | 0.082 | 0.082 | 0.082 | 0.082 | 0.082 | 0.082 | 0.082 |
| 4,0 | 0.063 | 0.063 | 0.063 | 0.063 | 0.063 | 0.063 | 0.063 | 0.062 | 0.062 | 0.062 |
| 4,5 | 0.049 | 0.049 | 0.049 | 0.049 | 0.049 | 0.049 | 0.049 | 0.049 | 0.049 | 0.049 |
| 5,0 | 0.040 | 0.040 | 0.040 | 0.040 | 0.040 | 0.040 | 0.040 | 0.040 | 0.040 | 0.040 |
| 5,5 | 0.033 | 0.033 | 0.033 | 0.033 | 0.033 | 0.033 | 0.033 | 0.033 | 0.033 | 0.033 |
| 6,0 | 0.028 | 0.028 | 0.028 | 0.028 | 0.028 | 0.028 | 0.028 | 0.028 | 0.028 | 0.028 |
| 6,5 | 0.024 | 0.024 | 0.024 | 0.024 | 0.024 | 0.024 | 0.024 | 0.024 | 0.024 | 0.024 |
| 7,0 | 0.020 | 0.020 | 0.020 | 0.020 | 0.020 | 0.020 | 0.020 | 0.020 | 0.020 | 0.020 |

Table 3.2 : g(r) at different distance from IBt, calculated with MC.
Difference with Reniers[19] are shown for validation.
Shown uncertainties were calculated taking into account the MC statistics only.

| Distance (cm) | g(r) | g(r) (Reniers) | Difference (%) |
|---|---|---|---|
| 0.5 | 1.018±0.002 | 1.014 | 0.38 |
| 1.0 | 1.000±0.003 | 1.000 | 0.00 |
| 1.5 | 0.940±0.003 | 0.939 | 0.12 |
| 2.0 | 0.863±0.003 | 0.861 | 0.24 |
| 2.5 | 0.784±0.003 | 0.778 | 0.80 |
| 3.0 | 0.701±0.003 | 0.696 | 0.73 |
| 3.5 | 0.623±0.003 | 0.621 | 0.20 |
| 4.0 | 0.552±0.003 | 0.549 | 0.46 |
| 4.5 | 0.486±0.003 | 0.486 | 0.00 |
| 5.0 | 0.425±0.003 | 0.427 | -0.50 |
| 5.5 | 0.369±0.003 | 0.373 | -1.05 |
| 6.0 | 0.321±0.002 | 0.320 | 0.50 |
| 6.5 | 0.285±0.002 | 0.277 | 2.68 |
| 7.0 | 0.243±0.002 | 0.240 | 1.15 |

The anisotropy function was calculated with equation 2.5, using the MC results at diverse angles θ. Our results are shown in tables 3.3 and 3.4 and in figure 3.5. Differences with Reniers[19] are on average -1.4 %, with a maximum difference of -9.4 % (again, a positive sign on the difference indicates an overestimation and a negative sign indicates an underestimation compare to Reniers). Here, the

differences between our results and Reniers's are due mainly to the MC statistical uncertainty but the difference of scoring regions at 90° also have and impact since the anisotropy function is normalised at that angle. The large differences occur at 0 degrees (i.e. on the longitudinal axis of the seed), close to the seed. On that axis, the statistical uncertainty is important because of the smaller amount of radiation emitted in that direction. Reniers reports a 14% statistical uncertainty at 5 cm on the longitudinal axis. In view of the large statistical uncertainty along the longitudinal axis of the seed where the large differences with Reniers are, those differences are considered acceptable.

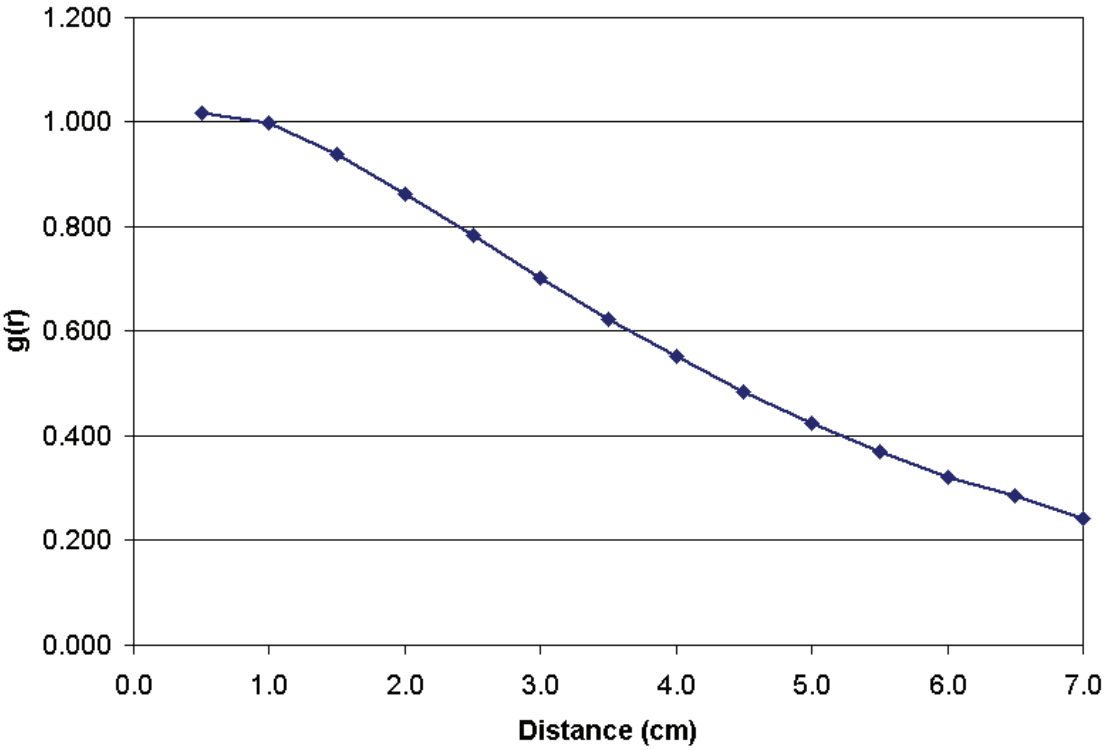


Figure 3.4 : Radial dose function versus distance, for IBt seed.

$$g(r) = 1.66522\text{E-}4r^5 - 3.98412\text{E-}3r^4 + 3.70014\text{E-}2r^3 - 1.54382\text{E-}1r^2 + 1.27856\text{E-}1r + 9.89977\text{E-}1 \quad (3.8)$$

Table 3.3 : F(r,θ) around an IBt seed. Shown uncertainties are calculated using only the MC statistical uncertainty.

| Θ<br>r(cm) | 0 | 10 | 20 | 30 | 40 | 50 | 60 | 70 | 80 |
|---|---|---|---|---|---|---|---|---|---|
| 0.5 | 0.487±0.006 | 0.742±0.002 | 0.838±0.002 | 0.892±0.002 | 0.949±0.002 | 0.978±0.002 | 0.994±0.002 | 0.997±0.002 | 0.993±0.002 |
| 1.0 | 0.508±0.007 | 0.684±0.003 | 0.785±0.003 | 0.848±0.002 | 0.908±0.002 | 0.950±0.002 | 0.980±0.002 | 0.992±0.002 | 0.997±0.002 |
| 1.5 | 0.561±0.008 | 0.691±0.003 | 0.784±0.003 | 0.847±0.003 | 0.906±0.003 | 0.9470.003± | 0.977±0.003 | 0.991±0.003 | 0.998±0.003 |
| 2.0 | 0.592±0.009 | 0.706±0.004 | 0.796±0.004 | 0.851±0.003 | 0.906±0.003 | 0.945±0.003 | 0.975±0.003 | 0.990±0.003 | 0.998±0.003 |
| 2.5 | 0.63±0.01 | 0.714±0.004 | 0.791±0.004 | 0.850±0.005 | 0.905±0.004 | 0.947±0.004 | 0.972±0.004 | 0.988±0.004 | 0.993±0.004 |
| 3.0 | 0.63±0.01 | 0.725±0.005 | 0.797±0.005 | 0.854±0.004 | 0.909±0.004 | 0.949±0.004 | 0.974±0.004 | 0.990±0.004 | 0.997±0.004 |
| 3.5 | 0.64±0.01 | 0.735±0.006 | 0.805±0.005 | 0.860±0.005 | 0.914±0.005 | 0.949±0.005 | 0.976±0.005 | 0.990±0.005 | 0.997±0.005 |
| 4.0 | 0.65±0.01 | 0.735±0.006 | 0.803±0.006 | 0.858±0.005 | 0.911±0.005 | 0.948±0.005 | 0.973±0.005 | 0.988±0.006 | 0.995±0.005 |
| 4.5 | 0.66±0.02 | 0.740±0.007 | 0.808±0.006 | 0.860±0.006 | 0.911±0.006 | 0.950±0.006 | 0.971±0.006 | 0.987±0.006 | 0.993±0.006 |
| 5.0 | 0.68±0.02 | 0.744±0.008 | 0.812±0.007 | 0.863±0.007 | 0.910±0.007 | 0.949±0.007 | 0.977±0.007 | 0.986±0.007 | 0.996±0.07 |
| 5.5 | 0.67±0.02 | 0.752±0.009 | 0.818±0.008 | 0.867±0.008 | 0.915±0.008 | 0.951±0.00 | 0.976±0.008 | 0.988±0.008 | 0.998±0.008 |
| 6.0 | 0.72±0.02 | 0.76±0.01 | 0.818±0.009 | 0.868±0.009 | 0.913±0.008 | 0.955±0.009 | 0.976±0.009 | 0.994±0.009 | 0.999±0.009 |
| 6.5 | 0.67±0.02 | 0.75±0.01 | 0.81±0.01 | 0.852±0.009 | 0.899±0.009 | 0.934±0.09 | 0.956±0.009 | 0.97±0.01 | 0.976±0.009 |
| 7.0 | 0.71±0.03 | 0.76±0.01 | 0.81±0.01 | 0.87±0.01 | 0.91±0.01 | 0.95±0.01 | 0.97±0.01 | 0.99±0.01 | 0.99±0.01 |

Table 3.4 : Comparison of F(r,θ) with the results of Reniers[19].

| Angle (degrees) | Distance | F(r,θ) | F(r,θ) (Reniers) | Difference (%) | Angle (degrees) | Distance | F(r,θ) | F(r,θ) (Reniers) | Difference (%) |
|---|---|---|---|---|---|---|---|---|---|
| 0 | 0.5 | 0.487 | 0.515 | -5.373 | 50 | 0.5 | 0.978 | 0.988 | -1.027 |
| | 1.0 | 0.508 | 0.554 | -8.378 | | 1.0 | 0.950 | 0.952 | -0.159 |
| | 2.0 | 0.592 | 0.656 | -9.713 | | 2.0 | 0.945 | 0.948 | -0.333 |
| | 3.0 | 0.627 | 0.681 | -7.963 | | 3.0 | 0.949 | 0.950 | -0.151 |
| | 5.0 | 0.68 | 0.703 | -3.544 | | 5.0 | 0.949 | 0.954 | -0.535 |
| 10 | 0.5 | 0.742 | 0.781 | -4.953 | 60 | 0.5 | 0.994 | 1.003 | -0.877 |
| | 1.0 | 0.684 | 0.711 | -3.837 | | 1.0 | 0.980 | 0.983 | -0.265 |
| | 2.0 | 0.706 | 0.712 | -0.865 | | 2.0 | 0.975 | 0.972 | 0.303 |
| | 3.0 | 0.725 | 0.737 | -1.601 | | 3.0 | 0.974 | 0.976 | -0.188 |
| | 5.0 | 0.744 | 0.752 | -1.004 | | 5.0 | 0.977 | 0.968 | 0.879 |
| 20 | 0.5 | 0.838 | 0.863 | -2.914 | 70 | 0.5 | 0.994 | 1.003 | -0.877 |
| | 1.0 | 0.785 | 0.795 | -1.224 | | 1.0 | 0.980 | 0.983 | -0.265 |
| | 2.0 | 0.796 | 0.792 | 0.442 | | 2.0 | 0.975 | 0.972 | 0.303 |
| | 3.0 | 0.797 | 0.811 | -1.748 | | 3.0 | 0.974 | 0.976 | -0.188 |
| | 5.0 | 0.812 | 0.818 | -0.737 | | 5.0 | 0.977 | 0.968 | 0.879 |
| 30 | 0.5 | 0.892 | 0.910 | -2.001 | 80 | 0.5 | 0.993 | 1.003 | -0.973 |
| | 1.0 | 0.848 | 0.860 | -1.411 | | 1.0 | 0.997 | 0.996 | 0.133 |
| | 2.0 | 0.851 | 0.852 | -0.156 | | 2.0 | 0.998 | 0.997 | 0.057 |
| | 3.0 | 0.854 | 0.860 | -0.754 | | 3.0 | 0.997 | 0.995 | 0.240 |
| | 5.0 | 0.863 | 0.854 | 1.035 | | 5.0 | 0.996 | 0.998 | -0.200 |
| 40 | 0.5 | 0.949 | 0.956 | -0.775 | | | | | |
| | 1.0 | 0.908 | 0.909 | -0.094 | | | | | |
| | 2.0 | 0.906 | 0.912 | -0.703 | | | | | |
| | 3.0 | 0.909 | 0.912 | -0.353 | | | | | |
| | 5.0 | 0.910 | 0.911 | -0.112 | | | | | |

In order to calculate the TG-43 dose at diverse points using Matlab, a fit was made using Excel for the anisotropy function at r = 1 cm in function of θ. The fit is expressed in equation 3.9. In figure 3.5, the anisotropy function is shown as a

function of θ, for different distances. The curves are fairly different for small values of θ. Consequently the choice to make the fit at 1 cm could be argued. A fit on the average over all distances might give better results. However, in that case the error would be higher close to the seed where it is important to have a good accuracy since the dose is higher. This is why we chose to make the fit relatively close to the seed.

$$F(\theta) = 8.6501\text{E-}7 \cdot \theta^3 - 2.03466\text{E-}4 \cdot \theta^2 + 1.66980\text{E-}2 \cdot \theta + 5.18545\text{E-}1 \qquad (3.9)$$

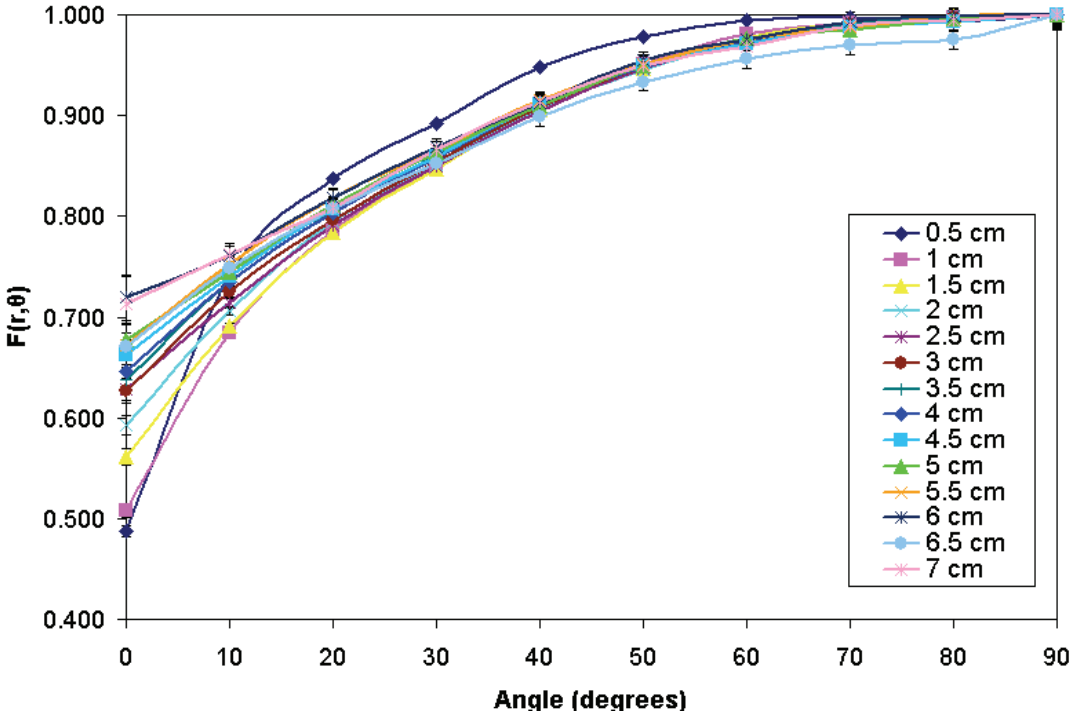


Figure 3.5 : Anisotropy function around an IBt seed, in function of angle.

Generally, in treatment planning, the values for F(r,θ) are interpolated from the tabulated value. Here, a fit was made in order to use Matlab for TG-43 calculations. For the angular component, the impact of fitting instead of interpolating was checked by comparing the results of the fit and linear interpolation for r = 1 cm for θ = 5, 15, 25, 35, 45, 55, 65, 75 and 75 degrees. The average difference was 0.2% with a maximum difference of 1.5%. The impact of making the fit at only one distace from the seed (1 cm) instead of interpolating from tabulated data at different distances from the seed is more important. The differences between the tabulated and fitted data are on average 3.5% and are higher for small angles and large

distances with a maximal difference of 38% at $0^o$, 6.5 cm from the seed where the dose is very small. At angles higher than $30^o$, the differences are less than 4%.

$S_k$ was determined by simulating a seed in air and scoring at a 30 cm distance, the scoring region reproducing the shape of the active volume of the WAFAC chamber which is used to measure $S_k$. The result of tally F6 (in MeV/g*particle) was corrected for attenuation, to obtain kerma in free space. For verification, simulations were also performed for a small scoring region of air in air and in free space, giving similar results (0.08% difference). $S_k$ was then calculated using equation 2.1 . The result, in MeV*cm2/g*particle, is used for the determination of $\Lambda$. Of course, for absolute dosimetry, the actual $S_k$ of the seed (in U) needs to be used. When we are interested in normalised dose, a value of 1 U is assumed for $S_k$.

For $\Lambda$, the seed was simulated in water, and the scoring was made in a 2 $mm^3$ cube at 1 cm from the seed. The result of the simulation (in MeV/g*particle) was divided by the value obtained for $S_k$ (in MeV*cm2/g*particle), giving $\Lambda$ in $cm^{-2}$ or cGy/U*h. We obtained $\Lambda$ = 1.009±0.007 cGy/U*h in water. A calculated value of 1.02±0.01 cGy/U*h was obtained by Reniers[19] . The difference of 0.011 (1.09 %) is within uncertainty.

In order to compare our MC results with measurements and TG-43 calculations, a conversion factor was determined in order to express the MC results (in MeV/g*particle) in dose rate per source strength unit. This was made by dividing the $\Lambda$ value by the result of the simulation at 1 cm in water, we obtained a factor of 3927 cGy/U*h(MeV/g*particle) ± 1.2%.

Hence, our simulation of the seed is validated by the comparison of g(r), F(r,θ) and $\Lambda$ with the results of Reniers[19].

For comparison of the interseed effect in different seed models, simulations were also performed for model 6711. To validate our simulations, the radial dose function at distances from 0.5 cm to 7 cm was calculated and compared with the consensus data from TG-43U1[16]. The average difference is -4.5% (the negative sign meaning that we are underestimating the results compared to TG-43U1) with a maximum difference of 9.0% at 4 cm. The statistical uncertainties on our simulation go from 0.3% at 0.5 cm to 6.9% at 7 cm. Again a 3% uncertainty due to the different

shape in scoring zone is considered. The reported MC uncertainties on g(r) in TG-43U1 are 2.5% at 1 cm and 5% at 5 cm. Hence, the difference between our results and the consensus data are within uncertainty.

The conversion factor from MC results to dose rate per source strength unit for 6711 model was calculated as 5435.9 cGy/U*h(MeV/g*particle). The calculated dose rate constant was 0.939 cGy/U*h, a difference of 2.7% with the consensus data of 0.965 cGy/U*h, again within uncertainty.

For the TG-43 calculations with model 6711, the consensus data published in TG-43U1 were used. The radial dose function and anisotropy function data were fitted giving :

$$g(r) = 8.19785\text{E-}5 \cdot \mathrm{r}^5 - 2.38317\text{E-}3 \cdot \mathrm{r}^4 + 2.52045\text{E-}2 \cdot \mathrm{r}^3 - 1.05876\text{E-}1 \cdot \mathrm{r}^2 + 2.16035\text{E-}3 \cdot \mathrm{r} + 1.07864 \quad (3.10)$$

$$F(\theta) = 5.81536\text{E-}7 \cdot \theta^3 - 2.22175\text{E-}4 \cdot \theta^2 + 2.21086\text{E-}2 \cdot \theta + 3.47455\text{E-}1 \quad (3.11)$$

### 3.2. Measurements in an acrylic breast phantom

Experiments were performed in a breast phantom, since breast treatment is a developing application of permanent LDR brachytherapy. Acrylic was chosen for the phantom because the radial dose functions in acrylic and breast tissue are similar, as will be shown in chapter 4. The phantom (figure 3.6) has a conic shape, and consists of 0.5 cm thick slices. Slots were made on the central slice to put the seeds. Thirty holes were made on a slice 0.5 cm from the central slice to put TLDs. Gafchromic films can be put between the slices. The phantom was positioned on a lung substitute phantom.

During the experiment the detectors were exposed for a time t and a dose $D(r,\theta)$ was measured at each point. The dose can be expressed as[9] :

$$D_m(r,\theta) = \frac{\dot{D}_0(r,\theta)}{\lambda}\left[1 - e^{-\lambda t}\right] \quad (3.12)$$

where $\dot{D}_o(r,\theta)$ is the initial dose rate and λ is the decay constant. Consequently, the initial dose rate can be expressed as :

$$\dot{D}_0(r,\theta) = D_m(r,\theta)\frac{\lambda}{\left[1 - e^{-\lambda t}\right]} \quad (3.13)$$

For an implant that would be left permanently, t=∞ and the total dose could be expressed as[9] :

$$D(r,\theta) = \frac{\dot{D}_o(r,\theta)}{\lambda} \tag{3.14}$$

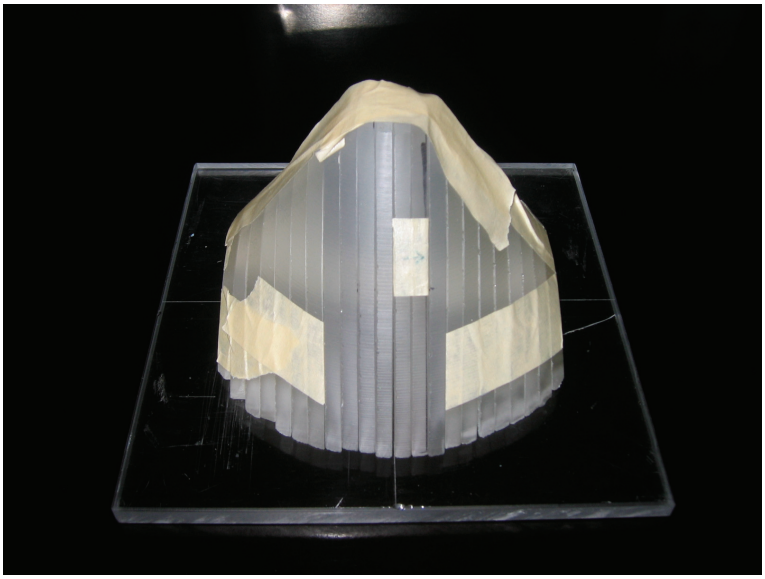

Figure 3.6 : Acrylic breast phantom.

### 3.3. TLD measurements

Thermo-luminescence dosimetry uses the property of some crystals (TLD) to trap electrons that have been freed by radiation and the holes associate to those electrons until sufficient energy is provided to liberate them. The energy is provided under the form of heat. When the pair is reunited, it emits phosphorescent light that can be measured to determine the dose deposited by the radiation that initially liberated the electron. The physics of such a process is described by McKinley's[32]. A material commonly used to make TLD is doped lithium fluoride (LiF).

#### 3.3.1. Dosimetric characteristics

TLD can have a small active volume. Because of the large dose gradients near LDR brachytherapy seeds, that characteristic makes TLD a good detector for measurements around those seeds. Also, the energy response can be quantified, so that difference between the calibration and measurement energies can be accounted

for. Finally, as reported in TG-43U1[16], for measurements of TG-43 parameters in LDR brachytherapy with 1 $mm^3$ LiF TLD, the statistical and systematic uncertainty can be lowered to 4 % and 7 % respectively (total uncertainty 7 % to 9 %), values inferior or equal to the recommended values of 5 % and 7 % respectively. Hence, in TG-43U1[16], 1 $mm^3$ LiF TLDs are considered as the dosimeter of choice for measurement of TG-43 parameters.

### 3.3.2. Measurement procedures

Measurements were made using 1 $mm^3$ TLD-100 from Harshaw. The TLDs were read with an automatic reader Harshaw SQ 5500. The heating treatments for experiment and calibration were similar, and the temporal treatment was as close as possible (the only discrepancy was in the exposure time since the experiment lasted for days). Pre-annealing was made one day before the beginning of exposure and the reading was made one day after the end of exposure. The pre-annealing as performed by heating the TLDs in an oven at 400$^oC$ for one hour. The reading parameters were the following : preheat at 125$^oC$ for 25 s and acquisition at 280$^oC$ for 23 s, with a temperature variation of 15$^oC$/s in between.

For calibration, the TLDs were given about 1 Gy, using a Theratron T-1000 $^{60}Co$ unit. The exact dose that was given to the TLDs was calculated every time depending on the output of the unit. The TLDs were read and the calculated given dose was divided by the reading (in nC), to determine a calibration factor (in Gy/nC) for each TLD. Hence, an unknown dose given to a TLD can be easily determined by multiplying the reading by the calibration factor. These procedures were initially repeated three times after stabilisation of the calibration factor. Twelve expositions were necessary for the factors to stabilise. The calibration was also redone regularly, the new calibration factor being the average between the old and the new results.

The linearity of the response was checked by exposing 5 TLDs at different doses (from 0.1 Gy to 3 Gy) with the $^{60}Co$ unit. An average calibration factor was calculated and compared to the average calibration factor for 1 Gy. The difference was inferior to ± 1 % up to 1.5 Gy and was higher than 2 % for 2 Gy and 3 Gy. Because of that, no measurement was made at more than 1.5 Gy.

At LDR brachytherapy energies, the exposure times are long (a few days to a few weeks), giving time to some electrons and holes to recombine before reading, hence causing a *fading* of the response. To check the extent of that fading, 20 TLDs were exposed to 1 Gy with the $^{60}$Co unit. Half were read the next day, half were read after 4 weeks. The difference between the average dose for both measurements normalised to the given dose was divided by the number of days between the measurements, giving a fading of – 0.14 % per day. This is negligible for exposures of a few days, but must not be ignored for longer exposures.

A set of five control TLDs was exposed to a known dose in the cobalt unit the day of the end of exposure and read with the TLDs used for the experiment, to correct for any variation due to the reader.

In order to be able to measure absolute dose with the TLDs, since the TLD calibration was made at $^{60}$Co energy while the measurements were made at $^{125}$I energy, an energy correction of 1.40±5% was used. That energy factor was also used by Reniers[19] who made an average of the factors obtained in various studies[29,33,34].

### 3.3.3. Uncertainty of TLD measurement

The statistical uncertainty for TLD was determined by calculating the average standard deviation of the calibration factors over four calibrations. That uncertainty was expressed in percent over the average measurement of all the TLDs for the four calibrations. This way, a statistical uncertainty of 3% was determined. A seed position uncertainty of 1.3 mm was taken as the quadratic sum of the maximal variations with the assumed ideal position, after measurement of the holes position and dimensions with a calliper. The position of TLD holes was measured and the measured position was used in the MC simulations, so only the uncertainty on that measurement was considered. However, like the seeds, the holes for the TLDs were larger than the TLDs so that the TLDs could have move a little in their holes. Also, a slight variation in slice thickness could have caused a position uncertainty. A TLD position uncertainty of 0.3 mm was taken as the quadratic sum of position uncertainties for the TLDs. A total position uncertainty of 1.3 mm was determined as

the quadratic sum of the position uncertainty for the seeds and the TLDs. Using the seeds radial function, a maximal gradient of 3%/mm was determined, so that a 1.3 mm position uncertainty correspond to a 4.0% uncertainty. A total uncertainty of 5.0% for relative measurements was taken as the quadratic sum of the statistical uncertainty and the position uncertainty.

The TLDs were calibrated in a $^{60}$Co beam. Any uncertainty in the dose given to the TLD would cause an uncertainty in the calibration factor. Dose measurements with a Markus chamber were made in three occasions and compared to the calculated dose. Measurements were made for different irradiation times. That way, an average uncertainty of 1.2% was taken as the calibration factor uncertainty. This uncertainty is a systematic error that will have an impact only on absolute dose measurements since it will be cancelled in the normalisation for relative dose. For absolute measurements, an energy correction of 1.40±5% was taken. The systematic uncertainty is then 5.1%, putting the total uncertainty for absolute dose to 7.2%.

## 3.4. Gafchromic® EBT measurements

### 3.4.1. General description

Radiochromic films (RCF) are transparent films that get bluer when exposed to radiation. The coloration is due to a chemical reaction when energy is transmitted from a photon or particle to a molecule, causing a polymerisation or the formation of a dye. Compared to regular radiography films, the RCF have the particularities of not requiring any particular processing, of being relatively insensitive to normal light and of having a composition closer to that of biological tissues[35]. However, they share with radiographic films the advantage of storing information for archival purpose (compared to TLD, for example, for which the dose can only be read once). Also, RCF have a good spatial resolution.

Because RCF are practical to use, appears to be relatively tissues equivalent and offers a good spatial resolution, these films (or at least the models sensible

enough at low energies) could be a very useful tool to measure dose distributions in LDR brachytherapy.

### 3.4.2. Dosimetric characteristics

Measurements were made with model Gafchromic® EBT. That model consists of two 17 µm active layers laminated on a 3 µm central surface layer and covered on each side by a 97 µm polyester, as illustrated on figure 3.7. Gafchromic® EBT was developed for IMRT applications. Its response is energy independent in MeV energies and its sensibility has been reported to diminish by less than 10 % in keV energies by Chiu-Tsao *et al.*[36] and on a white paper accessible on the company website[37]. According to the white paper, the Gafchromic® EBT offers a dose range going from 1 cGy to 8 Gy, a good uniformity (within 1.5 %) and a faster post-exposure development. There is no significant effect of fractionating the dose.

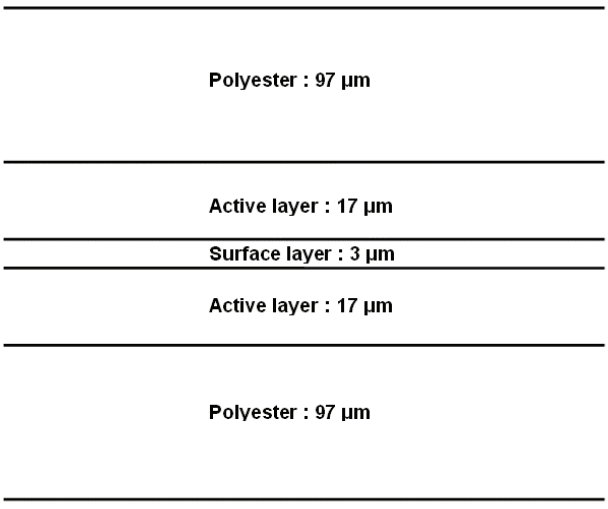


Figure 3.7 : Configuration of Gafchromic® EBT.

### 3.4.3. Measurement procedures

Gafchromic® EBT were read with a flat-bed scanner[38]. The films were put at the center of the scanner, using a template for reproducibility between the pre-exposure scan and the post exposure scan. The films were always scanned with the long axis of the film parallel to the long axis of the scanner. The red channel was

extracted to mach the maximal absorbency of the film. Before and after irradiation, each film was read five times. Five scans of an unexposed control film were made to take into account the large dependency of the reading on humidity and temperature, and five blank scans are also performed. A development time of at least 24 hours was left between the end of exposure and the reading. A Matlab program was used to analyse the readings. The *netOD* (net optical density) was determined as the difference between the OD read after and before exposure.

For calibration, pieces of film 1.5x2.5 $cm^2$ were exposed to different known doses at $^{60}Co$ and read. A *netOD* was determined for each dose. Then, a calibration curve (dose in function of *netOD*) was made and a fit of that curve permits to determine unknown doses using the *netOD*.

Measurements with Gafchromic® EBT were made for one and five seeds in the acrylic breast phantom by putting the film between the acrylic slices at 0 cm, 0.5 cm and 1 cm from the seeds. To help position the film in the phantom and the film center in the reading, marks were made on the phantom and on the film. Those marks were aligned when the films were put in the phantom and used in the Matlab program to situate approximately the film center. The film was then re-centred at the pixel with the higher signal.

### 3.4.4. Uncertainty of Gafchromic® EBT measurements

The statistical uncertainty for Gafchromic® EBT measurements was taken as the average standard deviation, expressed in percent, for the ratio NOD/given dose for three calibrations. The standard deviation was calculated for similar doses. That way, a 7% statistical uncertainty was calculated.

The exact positioning of the film inside the phantom was difficult, and so was the positioning of the exact film center during reading. To try to minimise the positioning error, the film was always centred at the pixel that had the higher signal. However, since there might be a variation of sensibility from pixel to pixel and since there might be a slight displacement between the reading before and after exposure, this solution is not ideal and might introduce another error. The film position uncertainty, including the slice thickness uncertainty, was taken as 1.5 mm. With the

1.3 mm uncertainty position, the total position uncertainty was estimated at 2.0 mm, which represents a 6.0% uncertainty.

The total uncertainty, calculated as the quadratic sum of statistical, and positioning uncertainties, is 9.2%.

### 3.4.5. Validation for LDR brachytherapy

The need for validation before using RCF for LDR brachytherapy dosimetry is due to the recommendations of TG-43U1[16] in which only TLDs and diodes are recognised as validated dosimeter. Also, dose-rate effect has been observed[39]. We verified the usability of Gafchromic® EBT films to measure the dose distribution around $^{125}$I LDR brachytherapy seeds in a phantom. Simulations and measurements were made using IBt. In every case, the films were placed in a plane parallel to the seeds. For this validation, it was first checked if the film introduces a perturbation in the dose. Then the dose rate effect was studied.

#### 3.4.5.1. Perturbation introduced by the film

Simulations were performed with MCNP4C, using the detailed physics treatment. For LDR brachytherapy energies, electrons are generally not transported in MC simulations. This assumption is permitted for the majority of detectors because the range of the electrons (around 17 µm for 30 keV electrons in water[28]) is small compared to the relatively large size of the scoring region. To simulate the dose deposition in the film (2 active layers of 17 µm), however, this assumption needs to be checked. To do so, we simulated the film at different distances from one seed, in a sphere of water. A unique scoring region was taken on the whole active layer of the film, in order to obtain good statistics. A pulse height tally (*F8) was used. The simulations were performed with and without electron transport. The results are given in table 3.5 . We can see that the difference is smaller than the sum of the uncertainties, except close to the seed (less than 2 mm), where cutting the electron transport introduces a small error inferior to 1.5 %. For both cases, the result of the calculation without electron transport is always higher than the result of the calculation with electron transport. Hence, the simulations can be carried out

without electron transport, particularly at large distance from the seeds, but care should be used when simulating a Gafchromic® film at less than 2 mm from a $^{125}$I seed. Since the relative difference is getting smaller as we go farther from the seed, the simulations were only performed up to 1 cm from the seed. For greater distances, it is assumed that the observed behaviour will continue and that not transporting the electrons will continue to have no impact.

Table 3.5 : Relative difference between doses calculated in the active layer of the Gafchromic® film for simulations without and with electron transport.

| Distance from the seed | Relative difference | Quadratic sum of uncertainties |
|---|---|---|
| 0.6 mm | 0.0138 | 0.0050 |
| 1 mm | 0.0131 | 0.0054 |
| 2 mm | 0.0102 | 0.0152 |
| 5 mm | 0.0076 | 0.0109 |
| 10 mm | 0.0040 | 0.0134 |

For this work, all other simulations with Gafchromic® EBT were performed with the films at 5 mm or more from the seeds, without electron transport. Also, a track length estimate of energy deposition tally (F4 or F6) was used.

The difference between calculations with and without electron transport is due to the variation in electron spectrum. The electron spectrum in one active layer of a film positioned at different distances from one seed was calculated with electron transport using a tally F4 with a tally energy card to separate the flux in energy bins going from 1.10E-03 MeV to 4.00E-02 MeV by 1E-0.3 MeV intervals. The electron spectrum for the film at different distances from the seed is shown in figure 3.8. We can see that very close to the seed, the spectrum is different and shows a higher proportion of electrons with energy slightly higher than 30 keV. The electrons of 30 keV and more have a range sufficient to leave the active layer without deposing their energy there. By not transporting the electrons and assuming a deposition of energy on the spot of their creation, these electrons would be assumed to deposit dose in the active layer and too big a dose would be calculated, as seen in table 3.5.

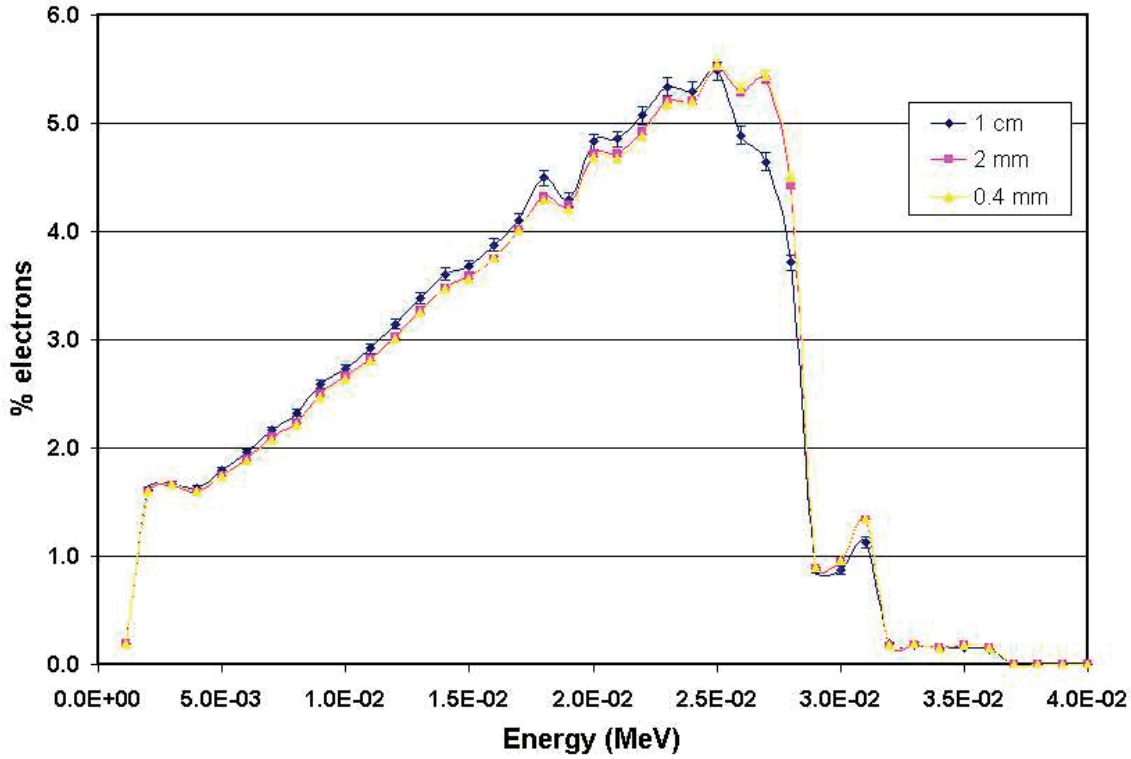


Figure 3.8 : Electron spectrum at different distance from one seed

To check if the film introduces a perturbation or if it measures the dose distribution adequately, simulations were performed for 9 seeds, in a sphere of water, with a film at 0.5 cm from the seeds, as illustrated in figure 3.9 .

The dose distribution was calculated in a lattice (2 mm by 2 mm pixels) on one active layer of the film. Then a calculation was performed, replacing the film by water. The dose distributions in Gafchromic® and water were then compared. Differences in pixels are all inferior to 2 %, with an average difference of 0.13%. Comparison of the isodoses distributions can be seen on figure 3.10a. Similar calculations with acrylic instead of water give similar results, with isodoses distributions showed in figure 3.10b. As we can see, Gafchromic® EBT film appears to be too thin to affect the dose at $^{125}$I energies. Hence, the MC simulations seem to demonstrate that Gafchromic® EBT could be used for dose distribution measurement around $^{125}$I LDR brachytherapy seeds in a tissue-equivalent phantom.

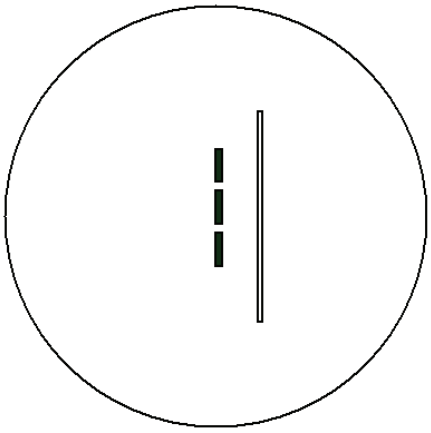

Figure 3.9 : Geometry for the simulation of a Gafchromic® EBT film near 9 seeds in a sphere of either water or acrylic.

We are not talking here of water equivalence since the film don't seems to introduce a perturbation either in water nor in phantom material which are not equivalent to each other at $^{125}$I energy. Actually, the Gafchromic® EBT is not equivalent at that energy. This can be seen by comparing the $\mu_{en}/\rho$, taken from the NIST website[28]. The $\mu_{en}/\rho$ of water is 1.55E-1 $cm^2/g$. The $\mu_{en}/\rho$ of Gafchromic® EBT is not given directly on the website and was calculated using the provided cross sections for the different interactions and assuming $\bar{g} = 0$. That way, a $\mu_{en}/\rho$ of 6.42E-2 $cm^2/g$ was obtained. Consequently, the film is not water equivalent, it is merely too thin to introduce a perturbation.

To check if there is a perturbation behind the film, we simulated films at 1 cm, on each side of 9 seeds in a sphere of acrylic with on one side a second film at 0.5 cm. A measurement was also made with 5 seeds in the acrylic breast phantom to check the absence of perturbation behind the films. The geometry is showed on figure 3.11. The isodose distributions are showed on figure 3.12. Difference is 1.2 % on average for the simulation and 4.3 % on average for the measurement.

Hence, Gafchromic® EBT in a plane parallel to the seed doesn't seem to introduce a significant perturbation in the measurement of dose distribution around $^{125}$I LDR brachytherapy seeds.

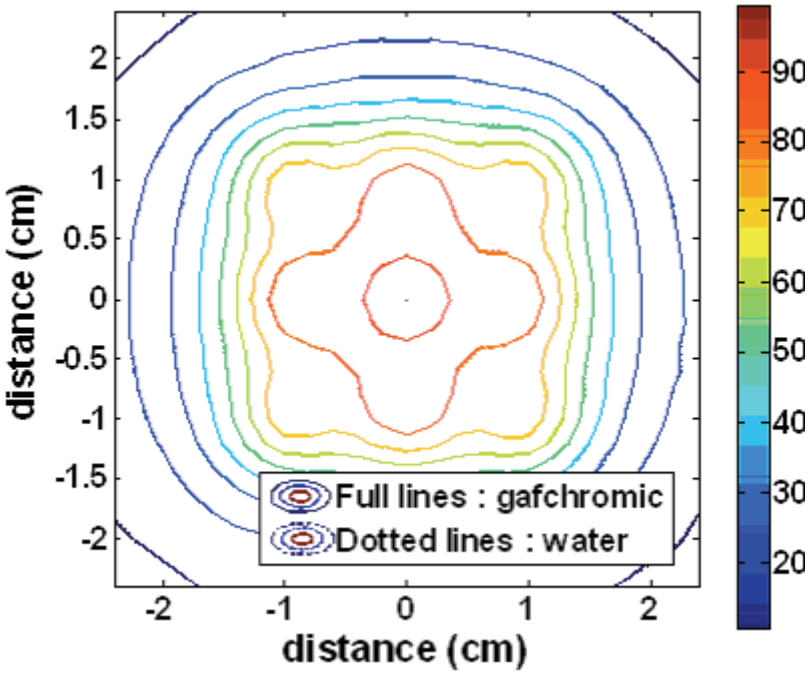


a)

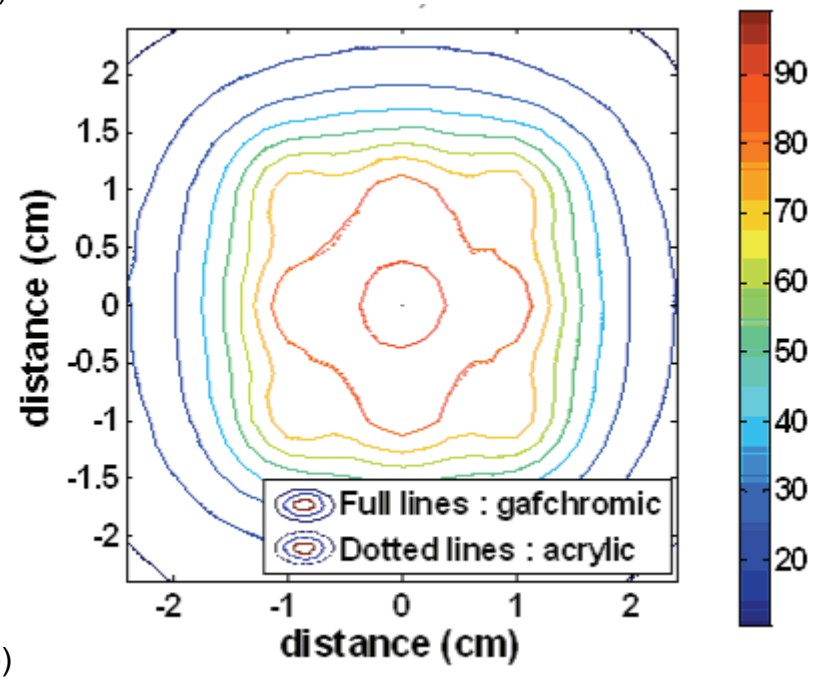


b)

Figure 3.10 : Comparison between the dose distribution, normalised to center in Gafchromic® and a) water for 9 seeds in water b) acrylic for 9 seeds in acrylic.

#### 3.4.5.2. Dose-rate effect correction

RCF are known to darken quickly in the first hours (up to a day) after the irradiation and to continue to darken slowly after that. Increases in responses of about 15% during the first day and of a few percents in the subsequent weeks have

been observed[39]. That response depends on the total dose, with a faster development for films exposed to lower doses. Because of that, it is important to match the *post-irradiation time* (the time between the end of exposure and the reading) of the experiment with that of the calibration. However, because of the long exposure necessary in LDR brachytherapy, a dose-rate effect is possible. Ali *et al.*[39] has studied the response in function of post-irradiation time of model Gafchromic® MD-55-2 exposed to diverse doses (1 Gy to 100 Gy) in one or two fractions, on a period of 90 days. Even if their results suggest that the overall dose-rate effect is small, they still observe an important dependency between dose response and total dose.

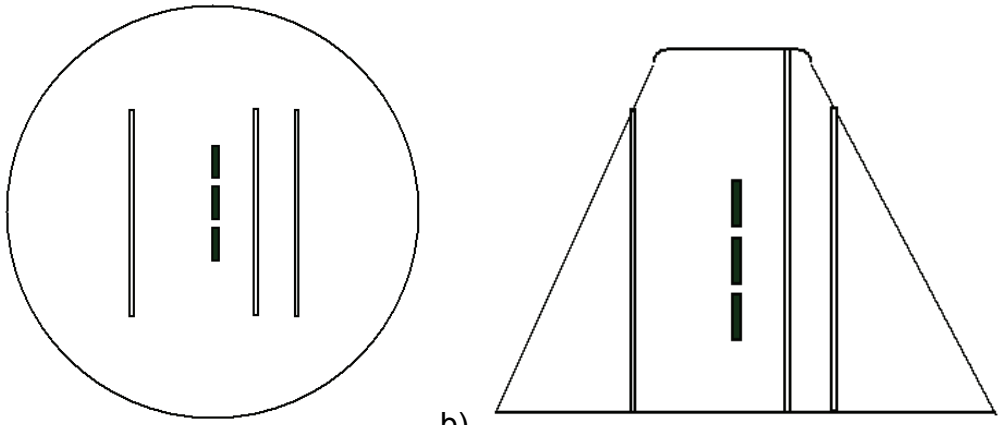


Figure 3.11 : Geometry for the study of perturbation behind Gafchromic® EBT film,
a) simulation with 9 seeds in a sphere of acrylic,
b) measurement with 5 seeds in the acrylic breast phantom.

To observe that dose rate effect, a piece of film was exposed with one seed in the acrylic breast phantom. The film was just beside the seed and the exposure lasted 15 days. The results were expressed as initial dose rate using equation 3.13. The dose was also calculated using MC. The simulation was made for the geometry of the experiment. The difference in percent between the measured and calculated dose is presented in function of measured initial dose rate on figure 3.13a. It can be seen that the dose is overestimated for small dose-rates. In the graph, the differences too close to the seed (the first 0.5 cm) are not shown since the dose given to the film to the first millimetres of film was higher than 8 Gy (out of the linearity region of the film).

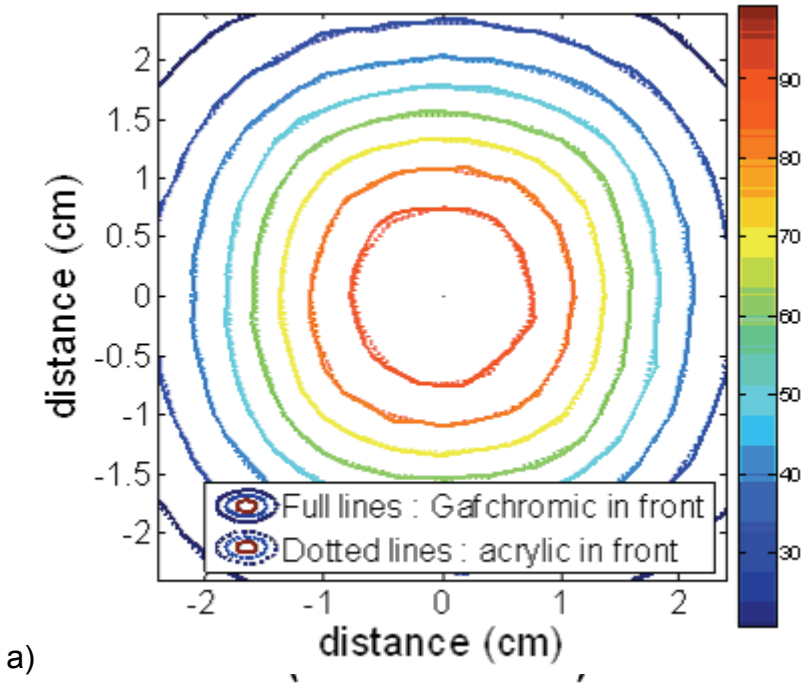


a)

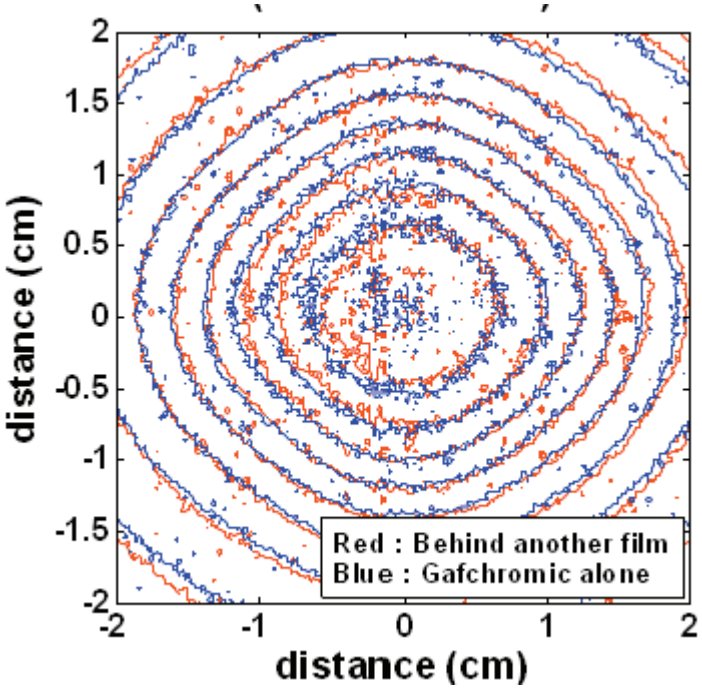


b)

Figure 3.12 : Perturbation behind Gafchromic® EBT film. a) MC calculation, with the isodoses normalised to center, b) measurement

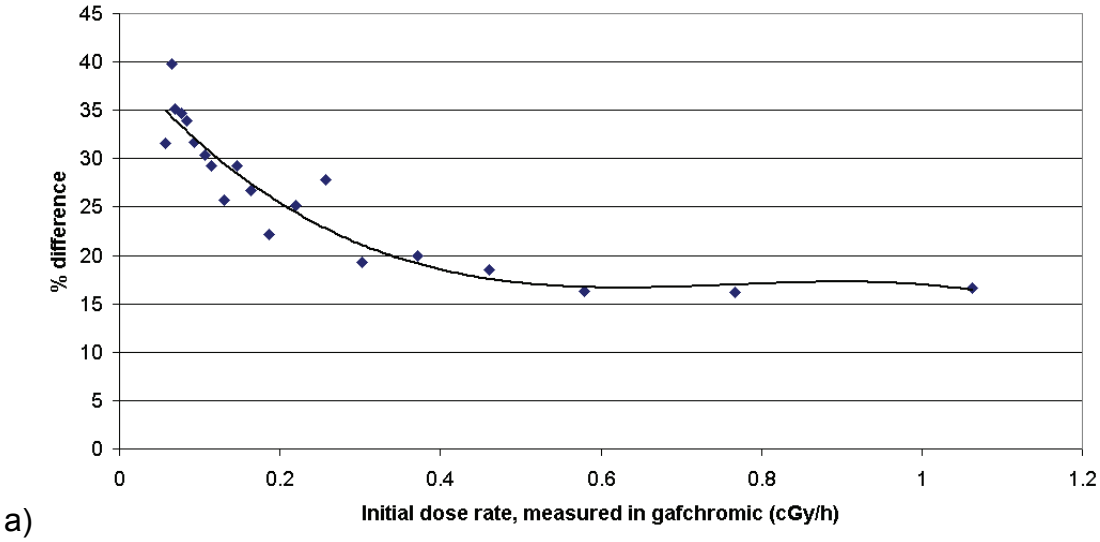


a)

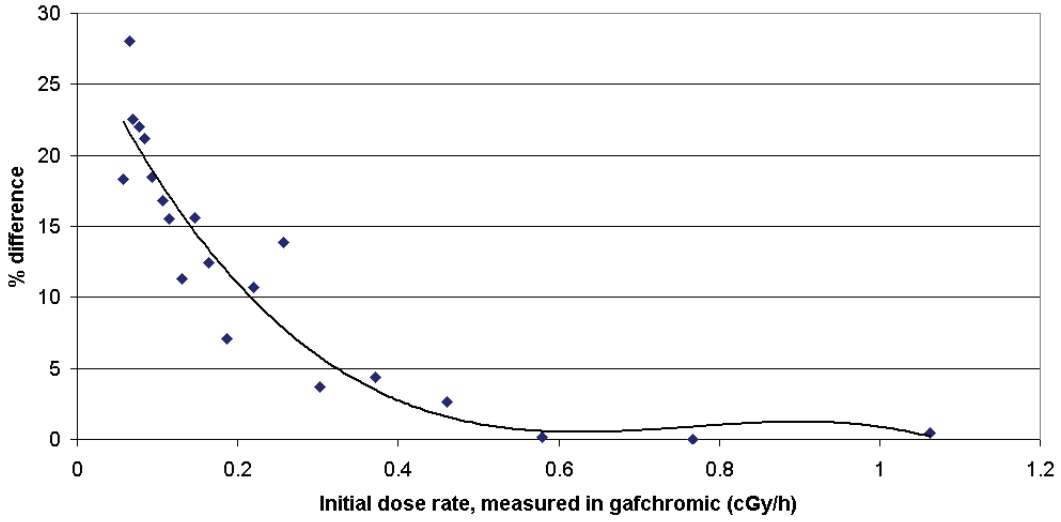


b)

Figure 3.13 : a) Percent difference between absolute dose measured with Gafchromic® EBT and calculated with MC in function of measured absolute initial dose-rate. b) Dose-rate effect versus measured absolute initial dose-rate. On figure b, the energy effect has been taken out so that only the dose-rate effect is shown.

A method was developed to correct for the observed dose-rate effect by expressing the difference in function of the dose-rate. The first 2 mm of the film where the electron transport would have an influence in the MC simulation is not considered since the first 5 mm were not considered and we were once again able to performed the simulation without electron transport.

Figure 3.13a shows the total difference in percent between measured and calculated dose versus dose rate. Figure 3.13b shows the part of the curve that is not constant with the dose rate, corresponding to the dose rate effect. The difference

that is constant with the dose rate was assumed to be due in totality to the energy effect. Note that this assumption might not be exactly true since the resulting energy correction of 16.3% would then be a little higher than the reported 10% between keV and MeV energy[27,28]. A fit was made of the dose-rate effect in function of measured dose-rate and was used to correct the measured dose in our Matlab program. All the Gafchromic measurements for the present work were corrected that way.

$$y = -68.952x^3 + 157.92x^2 - 116.62x + 28.535 \quad (3.15)$$

## 3.5. Methodology

### 3.5.1. Initial simulations

#### 3.5.1.1. Interseed effect

Calculations were performed, using MCNP4C to see how the interseed effect for model IBt compares to the interseed effect for model 6711 and how the platinum in model IBt influences the perturbation introduced by the seed. The simulations were performed for simple implant geometry with one, two and three seeds. The uncertainty for those initial simulations was calculated using MC statistical uncertainty only.

MCNP4C allows the use of a repetitive-structure function. Using this function, a structure can be created once and reproduced at other positions in the geometry. This is very useful in LDR brachytherapy studies because of the important number of seeds in an implant. The code allows the user to input the geometry of the seeds only once and then to positions as many seeds as he needs (in the limits of the computer capacity). That function was use for this study.

To study the interseed effect for IBt seed, we simulated one seed and superposed the results to see what we would have without the interseed attenuation, and three seeds together to take interseed attenuation into account, as schematised in figure 3.14. The simulations were made for seeds sharing the same transverse plane, with 0.5 and 1 cm separation, and for seeds sharing the same longitudinal axis, for 1 cm separation. For comparison, similar simulations were made for 6711

model. To have acceptable statistics far from the seeds and still have a good precision near the seeds, the scoring cells were made bigger, going farther from the seeds. The interseed effect was calculated using equation 2.9.

The IBt seed contains a platinum marker. The perturbation introduced by the platinum in model IBt is interesting to study since it is particular to that model. To study that effect, one seed was simulated with its platinum to take into account the self-attenuation of that seed. The seed was simulated alone and in the presence of an inactive seed with and without its platinum, to see how the platinum affects the attenuation due to that second seed. The second seed have to be inactive so that the radiation of that seed without the platinum doesn't affect the results. In other words, we are not interested in how the seeds self-attenuation is affected by the presence of platinum, but in how the platinum affects the perturbation by one seed of the radiation emitted by another. Because we studied the effect of an inactive seed, it is the perturbation factor that was calculated using equation 2.10.

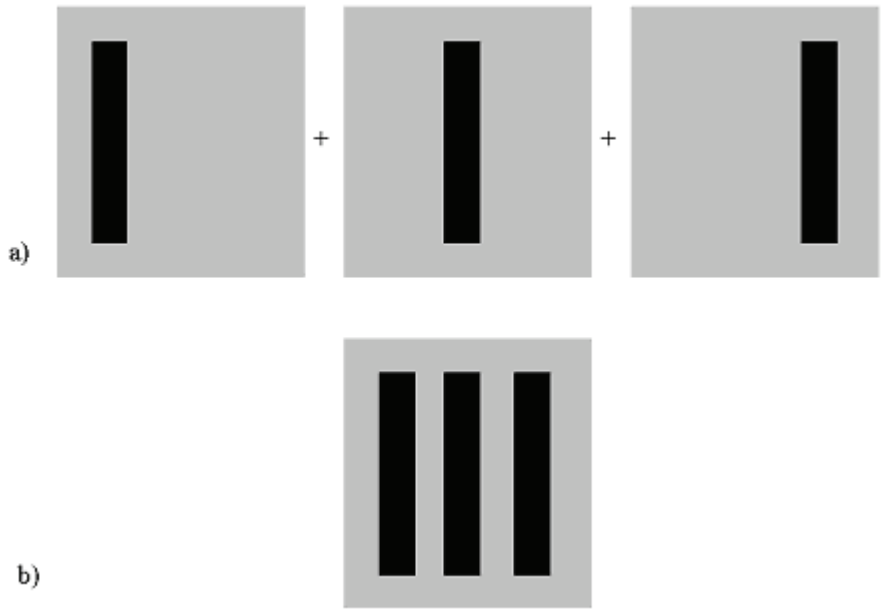


Figure 3.14 : MC simulation for the determination of the interseed effect.
a) superposition of the seeds simulated independently,
b) simulation of all the seeds together.

### 3.5.1.2. Tissue-composition effect

To study the tissue-composition effect, we have simulated a seed in different biological tissues and determined the radial dose function for each tissue, using the method described in chapter 3. As for biological tissues, the composition of phantom material will have an important impact on the dose distribution for experiment in LDR brachytherapy. Hence, in order to make measurements that are representative of reality, the phantom needs to be chosen carefully by matching its radial dose function with that of the tissue we want to represent. For this reason, simulations similar to those for tissues have been made for different phantom materials.

We chose to use the radial function to compare materials because, since we are comparing relative dose distribution in homogeneous phantom, we are mainly interested in the variation in attenuation in the material. Hence it is the radial dose function that will be mainly affected. The anisotropy function depends mostly on seed geometry and will not change a lot with the material. The dose rate constant might change a lot from one material to another, but since it is defined at a constant distance and independent of the point of measurement, the difference will be the same everywhere and the relative dose won't be affected. Of course, to calculate absolute dose in tissue or relative dose to tissues in an heterogeneous media, a correction would have to be made for the dose rate constant. Hence, a comparison of dose rate constant in different materials will also be presented. The dose rate constant in different material was calculated with MCNP4C. For the dose at 1 cm and $90^{o}$ in each material (except for water) the results of the simulation for the determination of g(x) was used. This means that the scoring region was a section of a sphere instead of a cube. It was checked by comparing the results of our simulations in water that the difference is only 0.5% between the results in the two shapes of scoring region.

For the simulations, the elemental compositions are from ICRU 44[40] , except for the prostate tissues for which the composition is given in ICRP technical report 23[41] and the RMI materials for which the elemental compositions were provided by the manufacturer[42].

To see if the difference compared to water is due mainly to the difference in density or elemental composition, we have simulate the seed in each material with water density, and the seed in water with the density of the materials.

### 3.5.2. Measurements in the acrylic breast phantom

TLD and film measurements were made in the acrylic breast phantom and compared with MC simulations results. In those simulations, the conic shape of the phantom was reproduced and filled with acrylic. The solid lung was reproduced under the cone and a sphere of air was simulated around that geometry. In order to simulate as best as possible the measurement geometry, the activity of the seeds was considered using the Sk given by the provider for the central seed and considering the relative Sk in the source definition card of our simulations. A maximal difference of –0.92% was obtained between the simulation accounting and not accounting for the exact activity of the seeds. The air in the holes around the seeds and in the unfilled holes was also simulated (with differences up to 5.5% between the simulations with and without the air), but because of possible movement in the holes, the simulations considering the air could only be an approximation. The repetitive-structure function was used for the MC simulation of the multi seed configurations.

#### 3.5.2.1. TLD measurements

Measurements were made in the acrylic breast phantom at 0.5 cm from a 5-seeds array plane. Because of the steep dose gradient, before the TLDs farther from the seeds received a significant dose the TLDs closer to the seeds were changed in order to receive no more than 1.5 Gy. An average between three measurements was taken.

In the MC simulations for TLD measurements, the scoring zones were cubes $1mm^3$ filled with TLD material to take into account the TLD attenuation and reproduce the experiment as best as possible. 100 000 000 particles were simulated.

The statistical uncertainty for the result of the simulation of the TLD measurement factor for each position was added to the uncertainty of the MC multiplication. Resulting uncertainty was on average 2.6% (maximum 4.3%). There is

air around the TLDs and seeds and in the unoccupied holes. Efforts were taken to simulate the air in the holes and around the seeds, but because of the position variation of the objects in those holes, the simulation can only be approximate. Air can also be present between the slices and at the phantom base, which will vary from one experiment to another and can't be simulated. An effort was also made to take into account the activity of the seeds. However, this activity was assumed isotropic in transverse plane of the seed. If a difference in activity was present from one side of the seed to the other, it was not possible to measure and consider it. These factors are difficult to quantify exactly, but it seems reasonable to estimate the total MC calculation uncertainty to 5%.

#### 3.5.2.2. Gafchromic® EBT measurements

Measurements were made with a Gafchromic® EBT film 0.5 cm from a 5-seeds array in the acrylic breast phantom (figure 3.15) and the results were compared with the results of the TLD measurements and MC simulations. Measurements were corrected for dose rate then normalised to the film center.

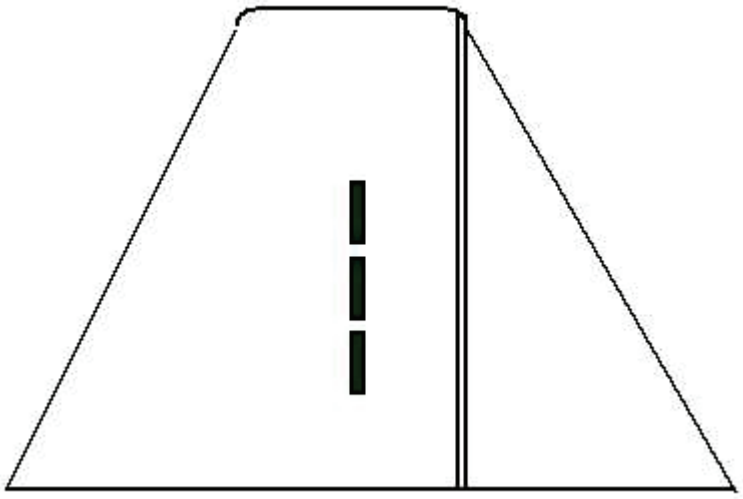

Figure 3.15 : Geometry for the measurement with Gafchromic® EBT film near 5 seeds in an acrylic breast phantom.

For the MC simulations, since it was shown that the films don't introduces a perturbation, the scoring zone was taken as a lattice in the acrylic. The width of the

lattice was the width of the surface layer and the two scoring zones. 100 000 000 particles were simulated. The average uncertainty for a simulation was 1.5%. With the uncertainties due to the simulation of the air in the seed holes, air between the slices and activity, the MC uncertainty is approximated to 4%.

### 3.5.3. Post implant study of realistic implants

Three models were used to study the impact of the interseed and tissue composition effects on the DVH for realistic implants. The first model is the TG-43 calculation. The second model is the MC calculation in water, taking into account the interseed effect. The third model is the MC calculation in tissue, taking into account the interseed and tissue composition effect. The MC simulations were made using the repetitive-structure function for the seeds. For the simulations in tissue, the dose to a small mass of water was scored. The three models were used to calculate the dose rate per source-strength unit at the center of each voxel in a lattice. Total dose was then calculated assuming an initial activity of 0.6 mCi (a typical value for prostate) and using equation 3.14.

Two realistic implants were studied, one for prostate treatment, one for breast treatment. The seeds position for those two implants were determined using post-implant data of actual treatment. For those two implants, the DVH for the PTV were calculated with TG-43, and with MC in water (to take into account the interseed effect) and in tissue (to take into account the tissue-composition effect). The seeds coordinates (determined based on CT images) for the 45-seeds prostate plan were provided by J.F. Carrier from CHUQ[43] in a private communication. The seed model used for this treatment was 6711, but for the present study purpose the plan was also studied using IBt Interseed$^{125}$. CT images of the 64-seeds breast plan was provided by J.-P. Pignol, from Sunnybrook Health Sciences Center[44] . Here, the actual treatment was performed with $^{103}$Pd seeds, but the present study was realised using $^{125}$I seeds, model IBt. Consequently, the implant that was studied in that case is an hypothetical implant since at our knowledge no breast permanent implant is performed with $^{125}$I.

For the first model, Matlab was used to calculate the dose rate per source-strength unit according to TG-43. The TG-43 parameters were determined using our MC results as described in chapter 3.

MC simulations were performed by simulating the seeds in either water (second model) or tissue (third model). The seeds were positioned using the coordinates determined on the post-implant images for the real treatments.

MC calculations were performed in a sphere of either water or tissues, and the results were scored in a 3D lattice. The size of the voxels was 1 $mm^2$ x 2.5 mm for the prostate implant (2.5 mm being the thickness of a slice). Because of the large size of the breast implant voxels of 2 $mm^2$ x 5 mm (5 mm being the thickness of a slice) were chosen in order to limit the calculation time.

The PTV contours were determined slice by slice (provided by Carrier[43] for the prostate implant and determined from the CT images for the breast implant[44]). An house-made Matlab program was used to determine the voxels from the lattice that were included inside the PTV. Those voxels were then sorted in interval of dose rates per source-strength unit and expressed as DVH.

For the interseed effect, a comparison was made between the DVH calculated with Matlab (TG-43 calculation not considering the interseed effect) and the DVH calculated with MC in water (taking into account the interseed effect).

For the tissue-composition effect, the DVH determined with MC in water and in tissue were compared.

# Chapter 4. Results

## 4.1. Initial simulations

### 4.1.1. Interseed effect

Results for the interseed effect for IBt model are shown in figure 4.1 and comparisons between the two models for 1 cm separation are shown in figure 4.2.

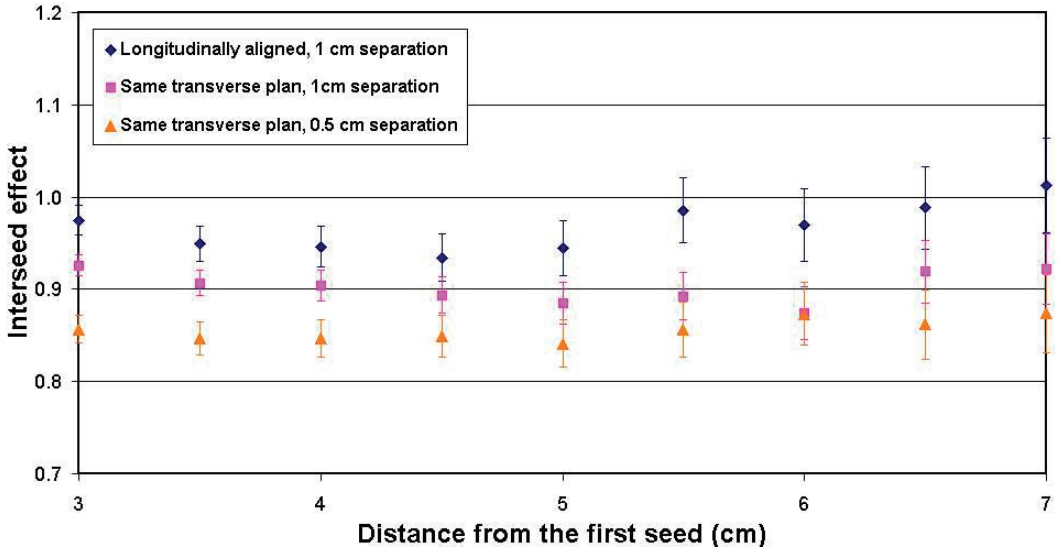


Figure 4.1: Interseed effect in function of distance for 3 seeds, IBt model.

As it was the case for Meigooni *et al.*[21] , we observed that the interseed effect is more important when the seeds share the same transverse plane than when they are longitudinally aligned. It is also more important when the seeds are closer one to the other. For seeds sharing the same transverse plane, the interseed effect is more important for model 6711 than for IBt. This is due to the silver rod in 6711 that absorbs more radiation that the air in IBt.

When the seeds are longitudinally aligned, as expected according to Meigooni *et al.*[21] , there is no significant interseed effect for 6711. However, there seems to be a small effect for the IBt model, up to 5 cm from the seeds since the error bars from model IBt don't reach an interseed effect of 1.0.

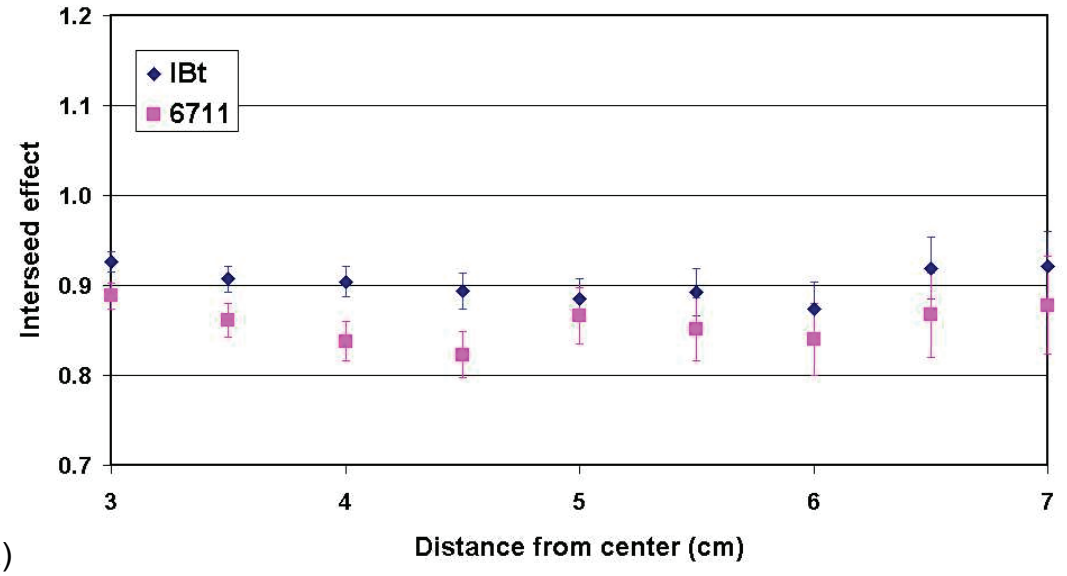


a)

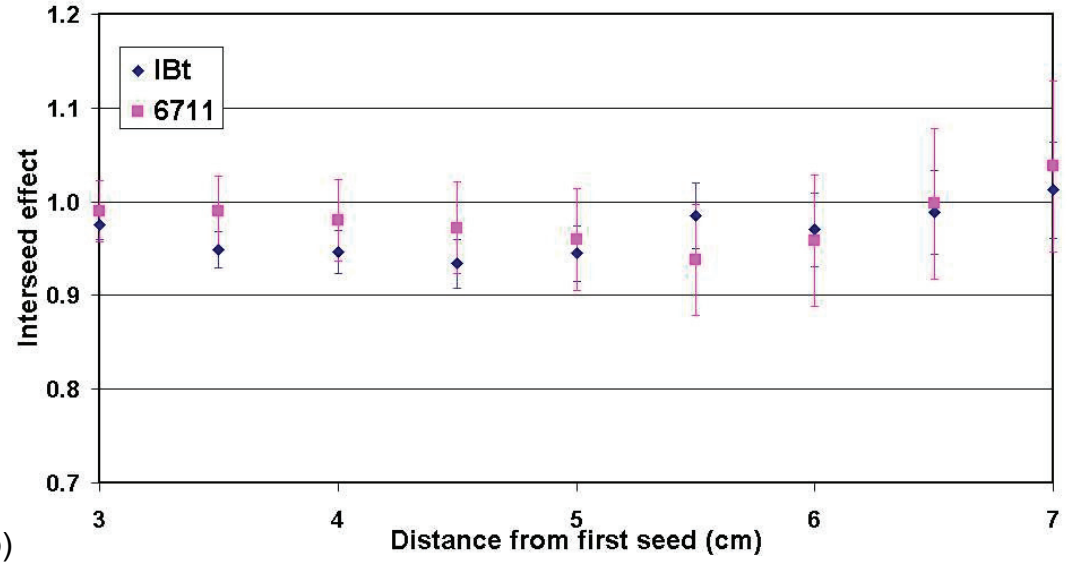


b)

Figure 4.2 : Comparison between the interseed effect in function of distance for seed models IBt and 6711 , a) for parallel seeds and b) for seeds longitudinally aligned. In both cases, the seeds were 1 cm apart.

An hypothesis to explain that result would be that the proportion of primary might be more important in the longitudinal direction for the IBt model than for 6711 model, leaving room for a perturbation which, as discussed earlier, affects mainly primary.

For the perturbation introduced by the platinum, results as a function of distance from the second seed are shown in figure 4.3. As expected, the second seed clearly introduces more perturbation when it contains platinum. However, with

the platinum, the factor is more important when the seeds are more distant, at least close to the seed. This is probably due to the actual geometry of the seed. The length of the platinum marker is smaller than the active length of the seed so that the platinum doesn't shield all the radiation. As view from a fixed distanced from the first seed, the proportion of the active length of that first seed that is shielded by the second seed is smaller when the seeds are closer, causing less perturbation.

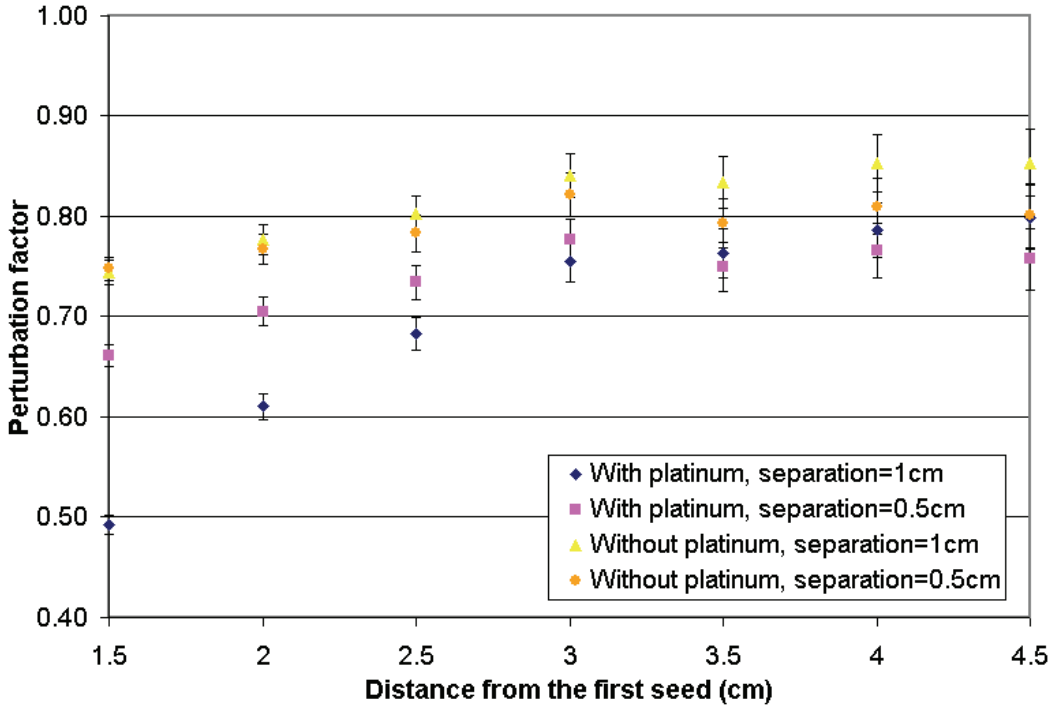


Figure 4.3 : Effect of the platinum on the perturbation factor.

### 4.1.2. Tissue-composition effect

Figure 4.4 presents the radial dose function in function of distance for diverse biological tissues, potential substitutes, and for water. We can see that, as expected, the results are very different. Table 4.1 presents the dose rate constant for water and for diverse biological tissues. These could be used if someone needed to calculate dose in tissue using TG-43. The correction could be made using the ratio $\Lambda_{tissue}/\Lambda_{water}$ .

Acrylic was chosen as a substitute for breast (2/3 mammal tissue, 1/3 adipose tissue) by matching their radial dose functions. This is shown on figure 4.5. Table 4.2 shows the composition of breast, acrylic and RMI454.

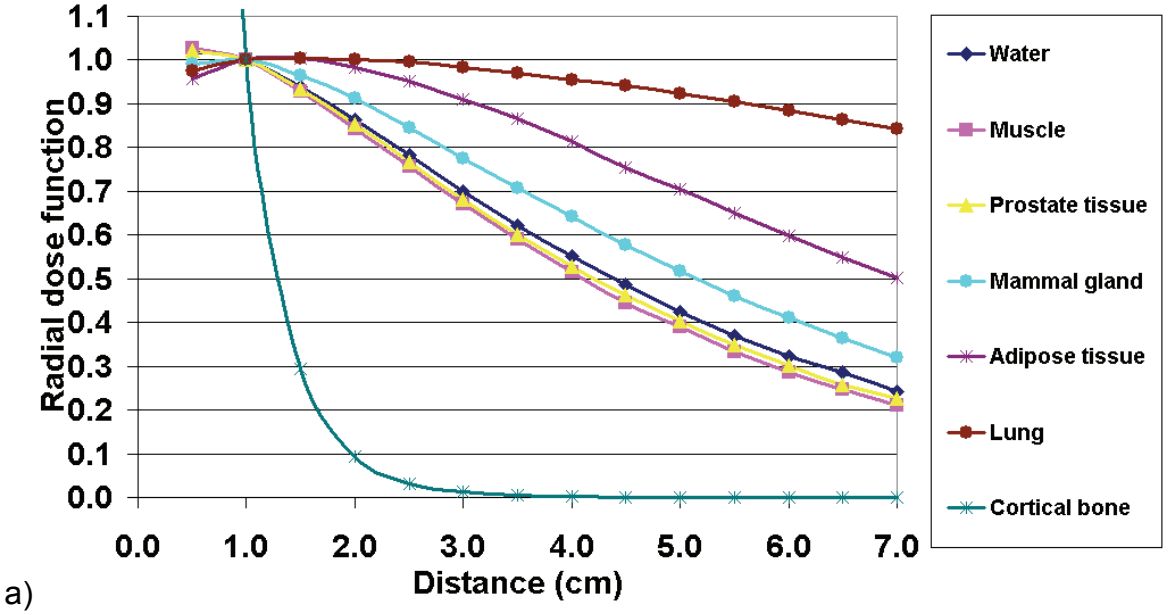


a)

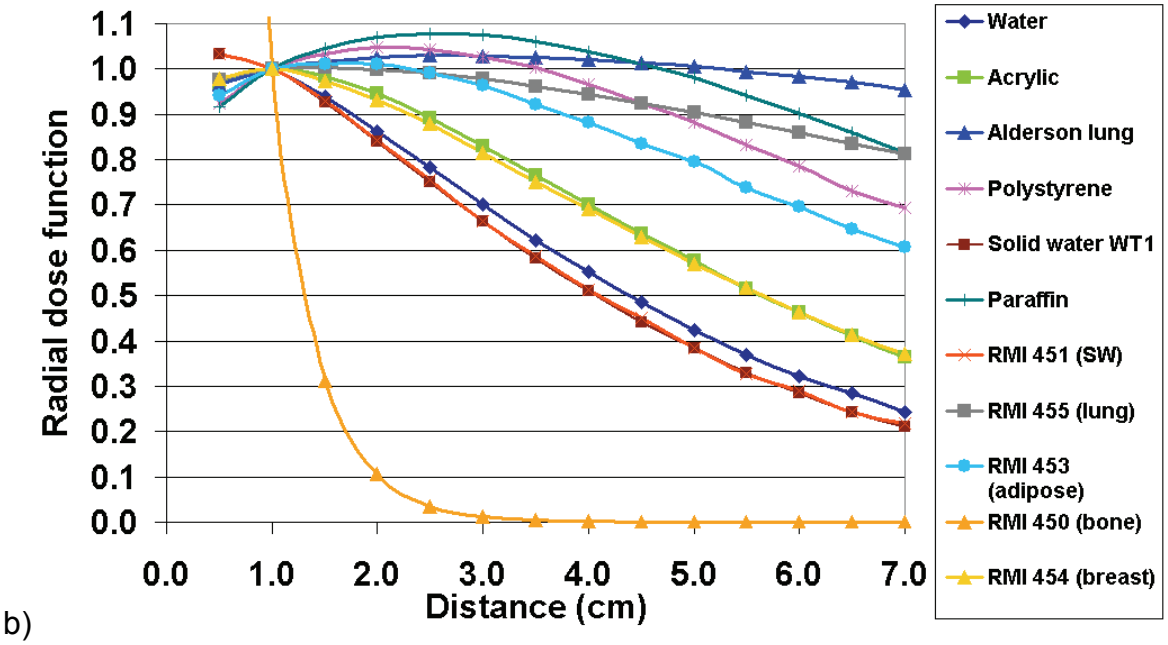


b)

Figure 4.4 : Radial dose function in function of distance,
a) for different biological tissues and b) for potential phantom materials.
Water is shown in both graphs, for comparison.

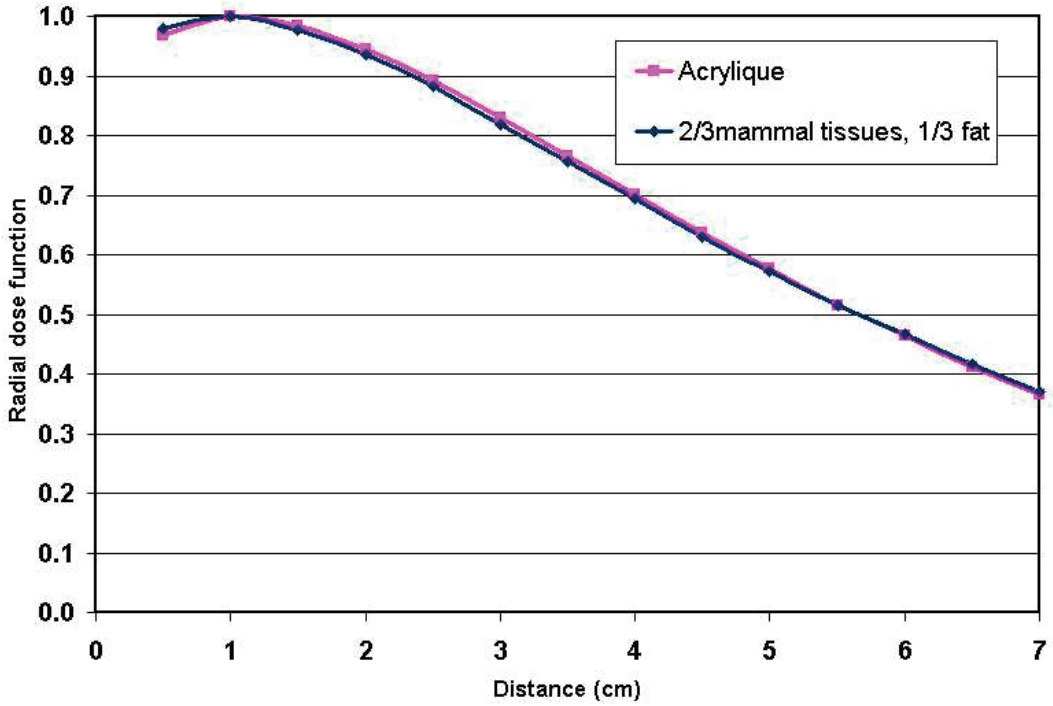


Figure 4.5 : Radial dose functions of breast tissue
(2/3 mammal gland, 1/3 adipose tissue), compared to acrylic.

Figure 4.6 to 4.10 show the results of the simulations in different materials with water density and in water with the material density . In general, the difference to water depends on both causes, but the dominant effect and relative importance of the effects depends on the material. For muscle and lung, the difference seems to be due mainly to the difference in density while for mammal gland, adipose tissue and bone it seems to be due mainly to the difference in tissue composition, even though the difference in density still have an important impact for bone.

Table 4.1 : Dose rate constant for various materials.

| Material | Λ |
|---|---|
| Water | 1.009±0.007 |
| Muscle | 1.022±0.003 |
| Prostate tissue | 1.000±0.003 |
| Mammal tissue | 0.848±0.003 |
| Adipose tissue | 0.669±0.003 |
| Cartilage | 1.166±0.003 |
| Cortical bone | 0.626±0.004 |
| Lung | 1.096±0.004 |

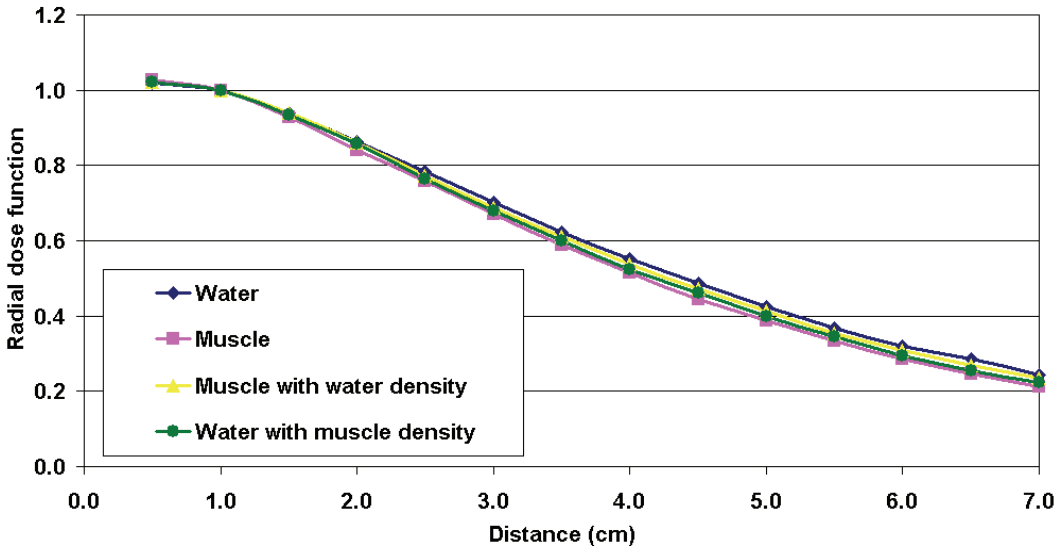


Figure 4.6 : Effect of the difference in elemental composition and density, compared to water for muscle.

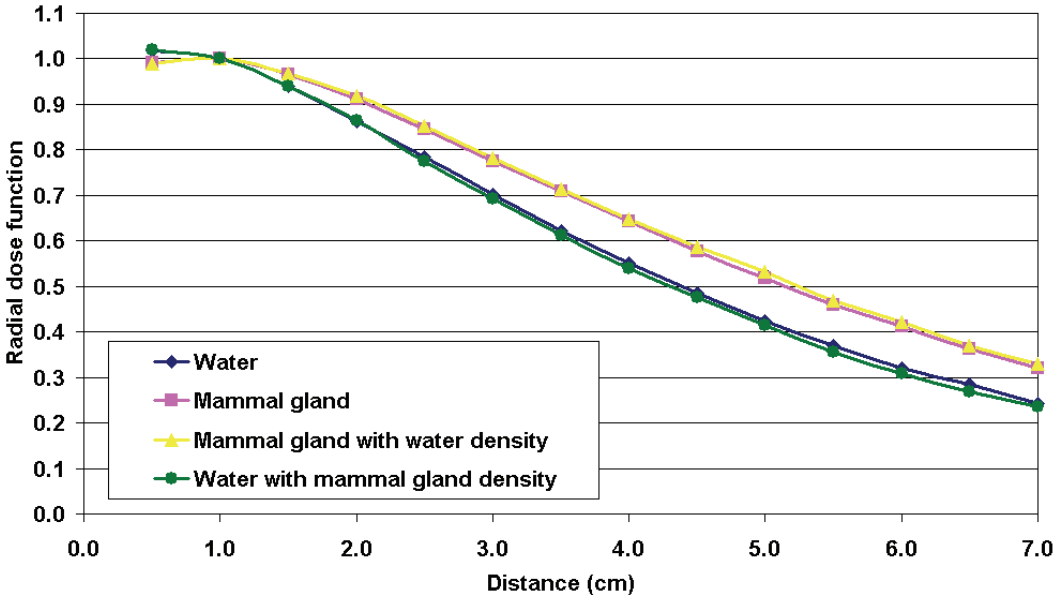


Figure 4.7 : Effect of the difference in elemental composition and density, compared to water for mammal gland.

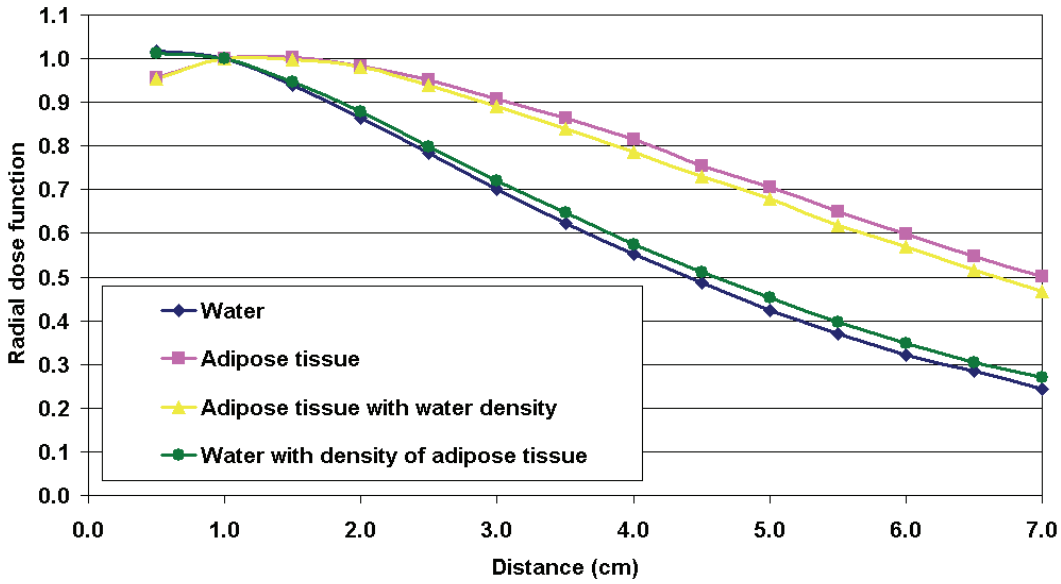


Figure 4.8 : Effect of the difference in elemental composition and density, compared to water for adipose tissue.

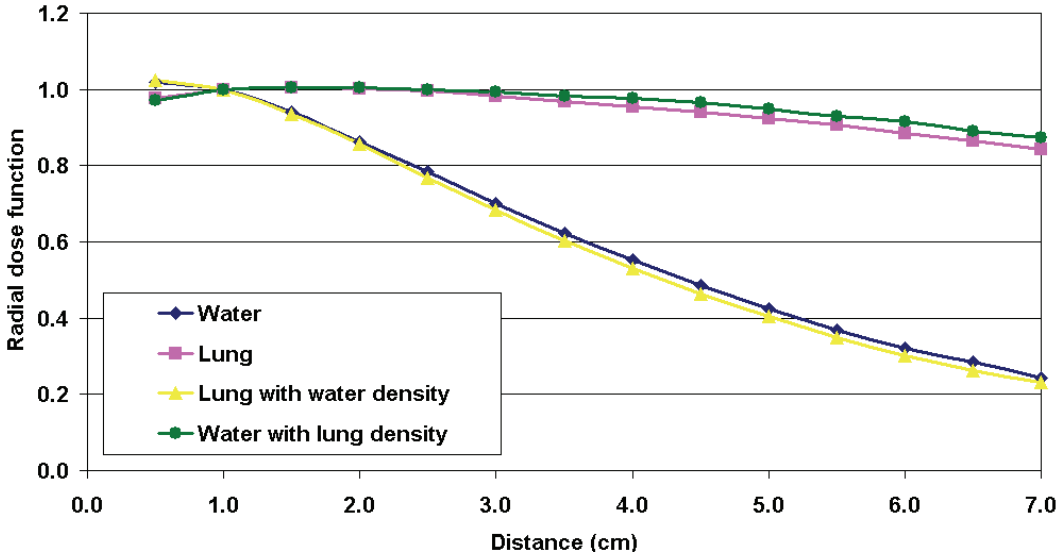


Figure 4.9 : Effect of the difference in elemental composition and density, compared to water for lung.

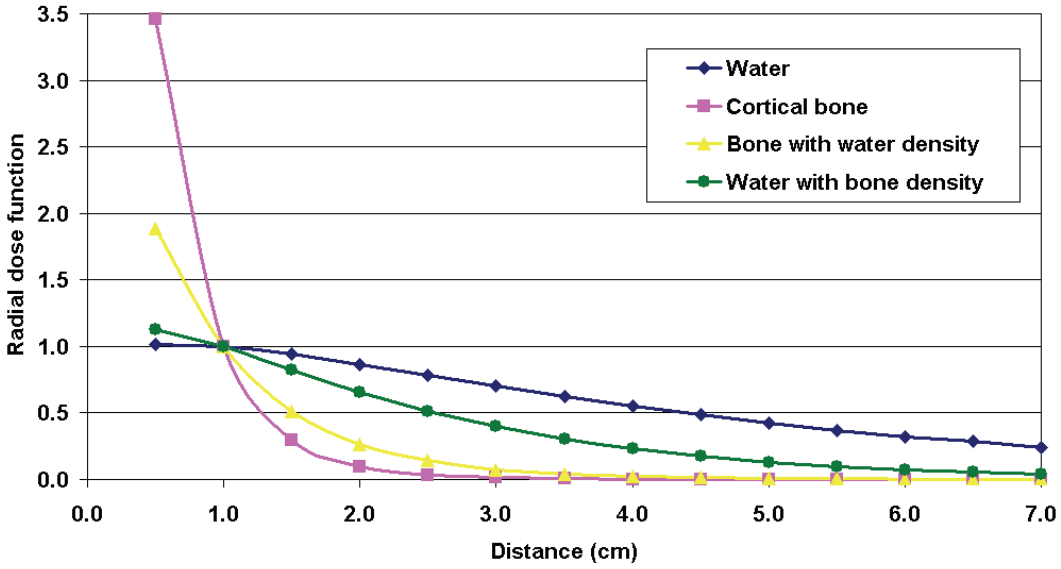


Figure 4.10 : Effect of the difference in elemental composition and density, compared to water for cortical bone.

Table 4.2 : Comparison of the composition of breast (2/3 mamal tissue, 1/3 adipose tissue)[40], acrylic[40] and RMI454[42]

| Material | H | C | N | O | Na | P | S | Cl | Ca |
|---|---|---|---|---|---|---|---|---|---|
| Breast | 10.87 | 42.07 | 2.23 | 44.40 | 0.10 | 0.06 | 0.17 | 0.10 | - |
| Acrylic | 8.00 | 60.00 | - | 32.00 | - | - | - | - | - |
| RMI454 | 8.59 | 70.11 | 2.33 | 17.90 | - | - | - | 0.13 | 2.31 |

## 4.2. Measurements in the acrylic breast phantom

### 4.2.1. TLD measurements

Differences between absolute doses measured with TLDs and calculated with MC are shown on figure 4.11. The average difference is –0.15 % and the maximum difference is 12.2 %. These results are within the uncertainties for measurement and simulation. Hence, we can say that our measurements validate our MC model.

### 4.2.2. Gafchromic® EBT measurements

Differences between the initial dose rates, normalised to centre position, measured with Gafchromic® EBT and TLDs are shown in figure 4.12 . The average difference is 2.4 %, with a maximal difference of 17.7 %. Here, the only measurement higher than the sum of uncertainty for both detectors is very close to

the base of the phantom, in a low region dose and where air gaps might have cause an error.

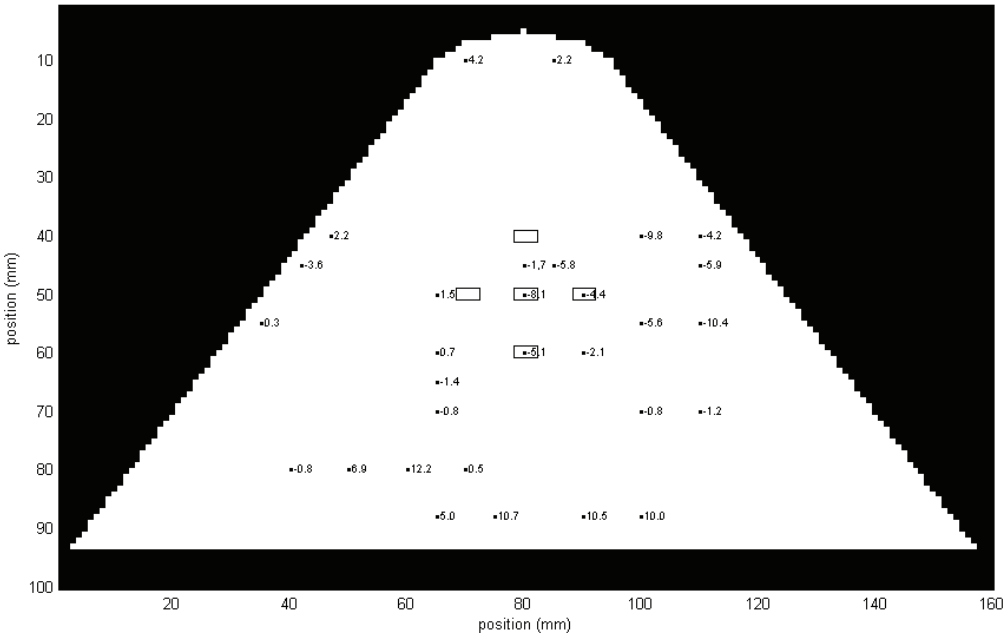


Figure 4.11 : Comparison between absolute dose determined with TLD measurement and MC simulations. The projected positions of the seeds are shown. Remember that the seeds are in a slice 5 mm apart from the TLDs.

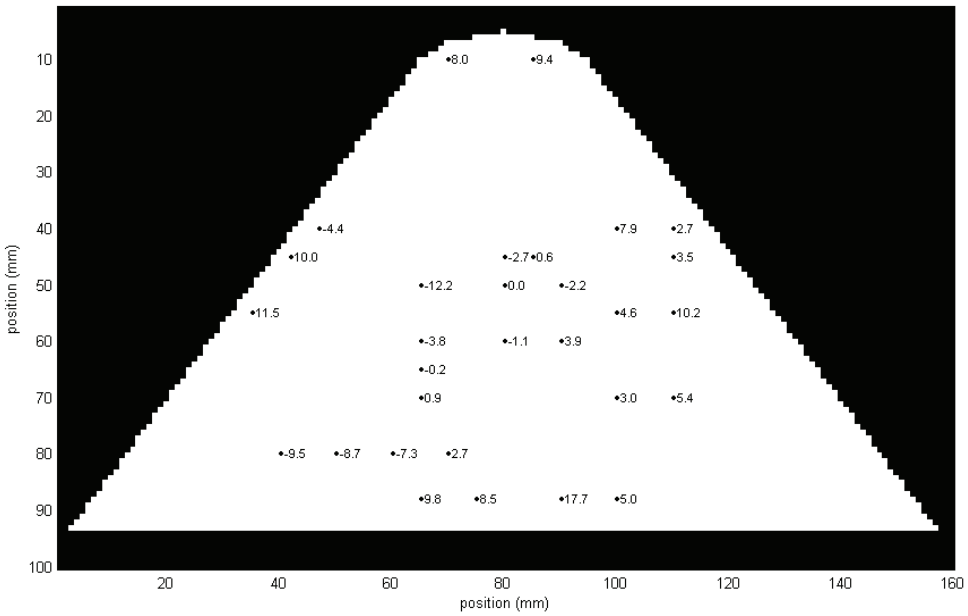


Figure 4.12 : Differences in percent between dose, relative to centre, measured with Gafchromic® EBT (corrected for dose-rate) and TLD measurements.

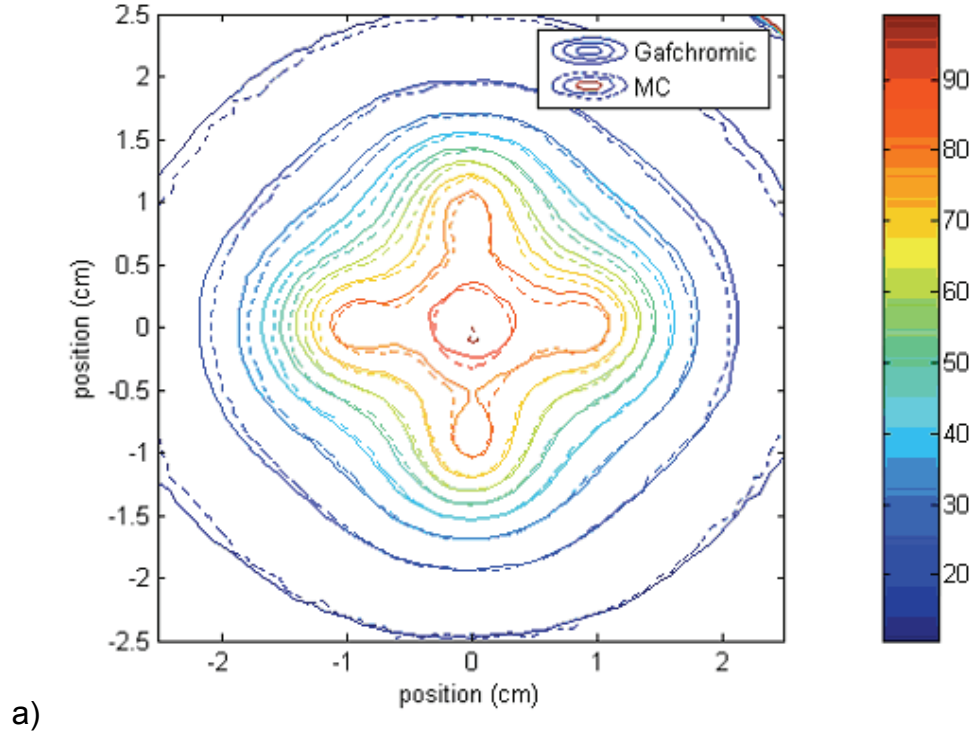


a)

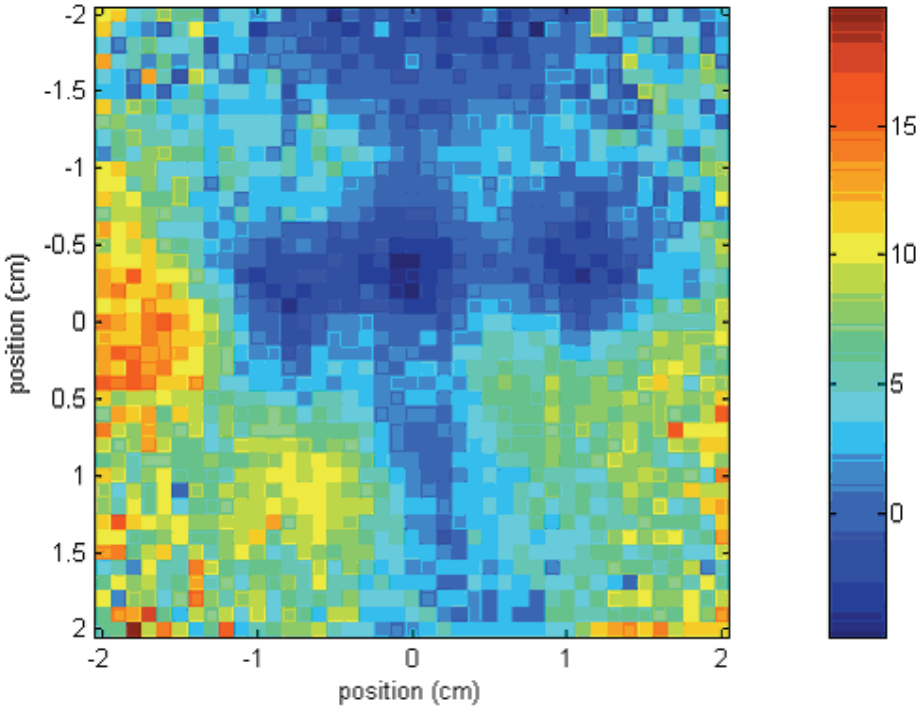


b)

Figure 4.13 : Differences, in percent, between relative doses (normalised to the centre of the film), measured with Gafchromic® EBT with the dose-rate correction and calculated with MC. a) isodoses, b) difference map in %. Because of the scanning direction, the base of the phantom is situated at the left of the figure.

Differences between the Gafchromic® EBT measurements and MC calculations for the same geometry are shown on figure 4.13. The isodoses are very similar, with a few discrepancies near the seeds, explained by the uncertainty of seed positioning. The average difference on the difference map of figure 4.13b is 4.2 %, with a maximal difference of 19.8 %. Here some pixels show differences higher than the sum of uncertainties for measurement and calculation. Again, most of those discrepancies are close to the base of the phantom and could be due to the presence of air gaps. The large differences are localised in a low dose region (the calculated dose is lower than 30% of the central dose).

## 4.3. Post implant study of realistic implants

### 4.3.1. Prostate plan

Results for the prostate plan are shown on figure 4.14 for the IBt seed and on figure 4.15 for the 6711 seed.

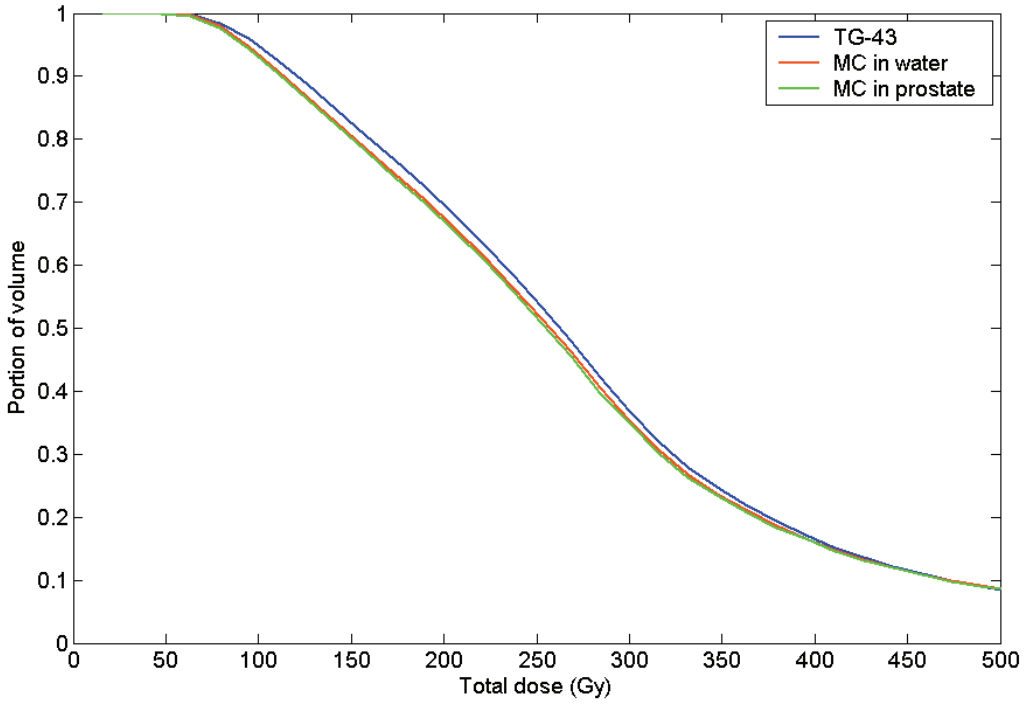


Figure 4.14 : Interseed and tissue-composition effect for a 45-seeds prostate implant, seed model IBt.

#### 4.3.1.1. Interseed effect

We can see on figure 4.14 and 4.15 that, as expected[25], the DVH is right-shifted by ignoring the interseed effect and making the dosimetry purely based on TG-43 with model IBt and 6711.

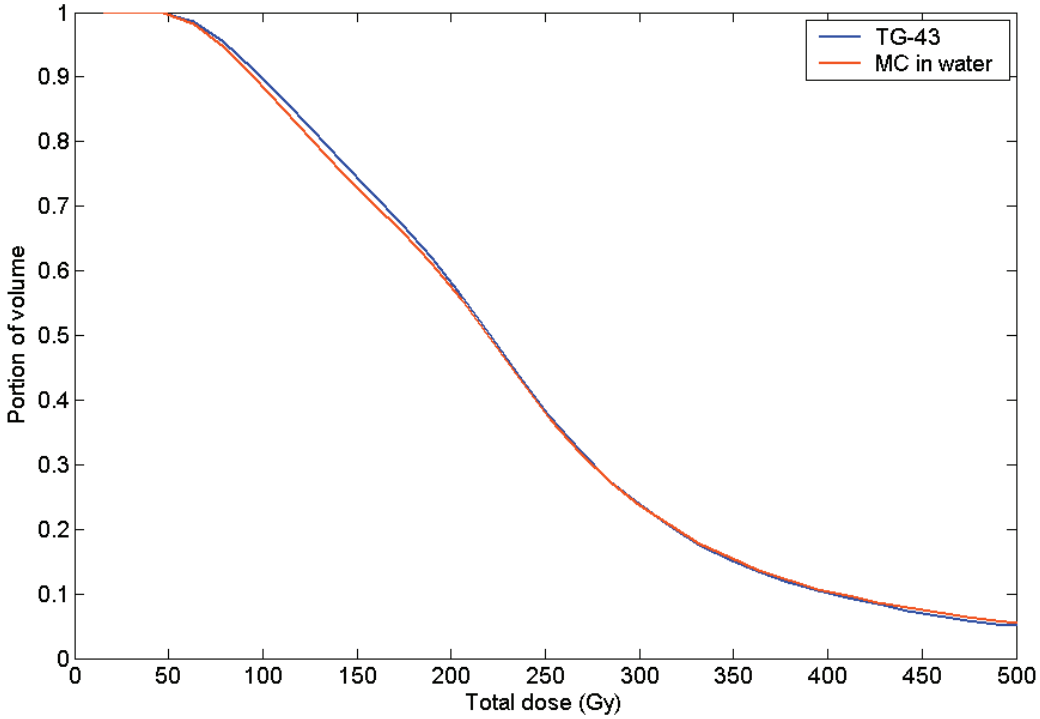


Figure 4.15 : Interseed effect for a 45-seeds prostate implant, seed model 6711.

The interseed effect that we observe is more important than what we could expect according to the pre-implant study of Carrier *et al.*[25] where a drop in D90 due to interseed effect of 1.2% was obtained for a low seed density of 1.62 seeds/cm$^3$ (42 seeds in a 26 cm$^3$ prostate) with seed model 6711. Comparatively, for a seed density of 1.10 seeds/cm$^3$ (45 seeds in a 41 cm$^3$ prostate), we obtained a drop in D90 of 6.3% for IBt model and 6.5% for the 6711 model. The effect is supposed to become less important for a lower seed density[25]. However, the results obtained by Carrier *et al.*[25] were for idealistic implant made with a treatment planning system. Our results are based on the study of a post-implant in which the seeds might have move. In the post implant study by Carrier *et al.*[26], for an average number of 52 seeds and an average prostate volume of 31 cm$^2$ (hence an average of

1.68 seeds/cm$^3$), the average drop in D90 due to interseed effect was 4.2%, higher than the 1.2% obtained for a pre implant[25] for a similar seed density. Hence, the movement of seeds seems to have an important impact on the interseed effect and might explain the high interseed effect we obtained. Also, the implant particularities have been showed to have a significant impact on interseed effect[25,26].

#### 4.3.1.2. Tissue-Composition effect

As expected[25], the DVH is also right-shifted by ignoring the tissue composition effect for a prostate implant. A slightly more important shift might be expected according to Carrier *et al.*[26] where a difference of 2.6% is reported between D90 for MC simulations in water and in prostate tissue. According to our results, the difference on the D90 is 1.6% due to the tissue composition effect. However, in Carrier *et al.* for the simulations in tissue, the dose to tissue was scored[26] while in our simulations the dose to a small mass of water was scored, as “dose-to-water” is still the standard in treatment planning system. This would obviously have an impact.

The effect of ignoring the tissue composition on dose distribution for a prostate implant is showed on figure 4.16. This figure presents the isodoses for the central slice in the 45-seed implant in a sphere of prostate tissue. As we can see, the isodoses don’t appear to be significantly shifted, at least for the particular configuration we studied.

### 4.3.2. Breast plan

For the breast implant, results are shown on figure 4.17.

#### 4.3.2.1. Interseed effect

For this implant, the expected right shift for the TG-43 calculation[25] is observed with a variation of 4.7% on the D90. This is smaller than the interseed effect we observed for the prostate implant, unsurprisingly since the seed density is smaller for the breast implant.

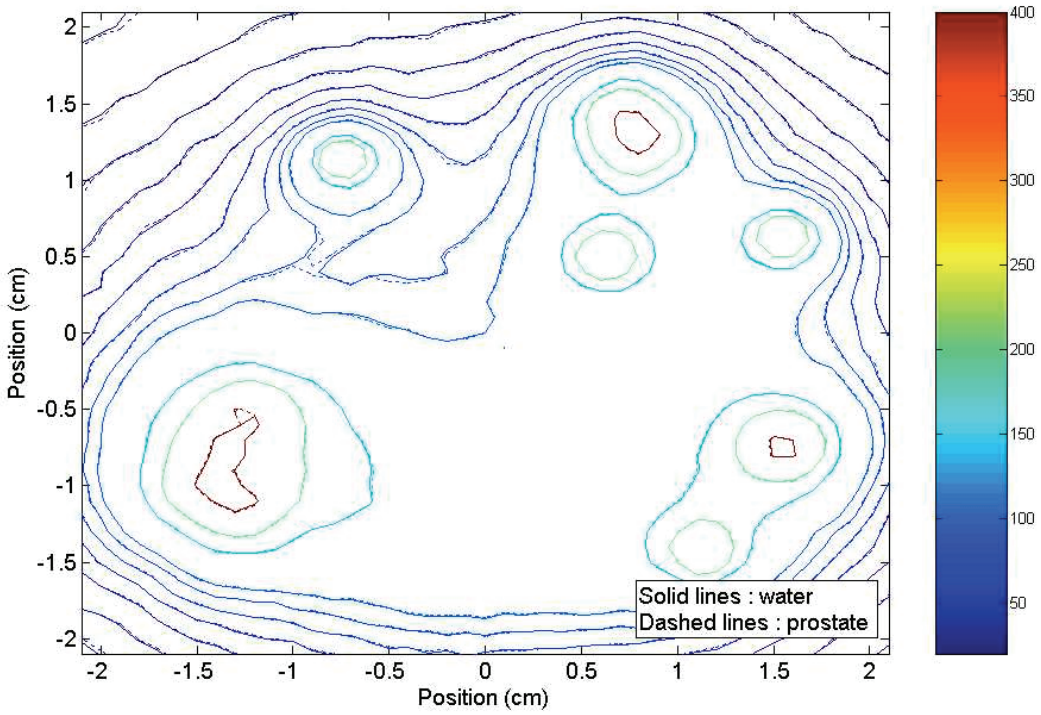


Figure 4.16 : Isodoses, normalised to centre, for the prostate implant in water and tissue.

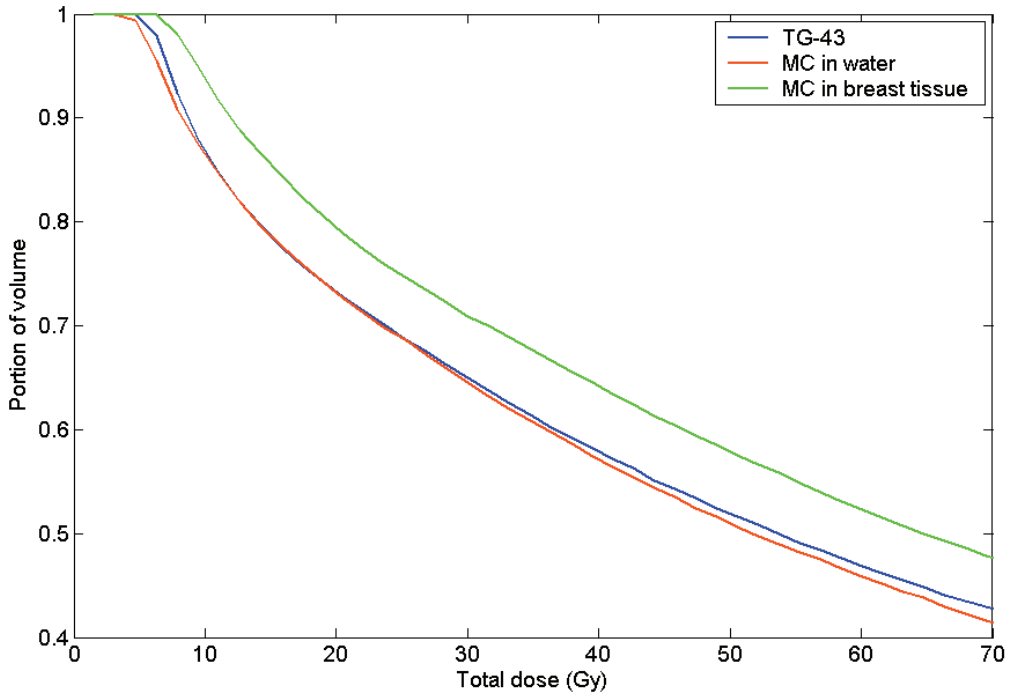


Figure 4.17 : Interseed and tissue composition for a breast implant, seed model IBt. Note that the total dose was calculated assuming typical source strength similar to that for a prostate implant.

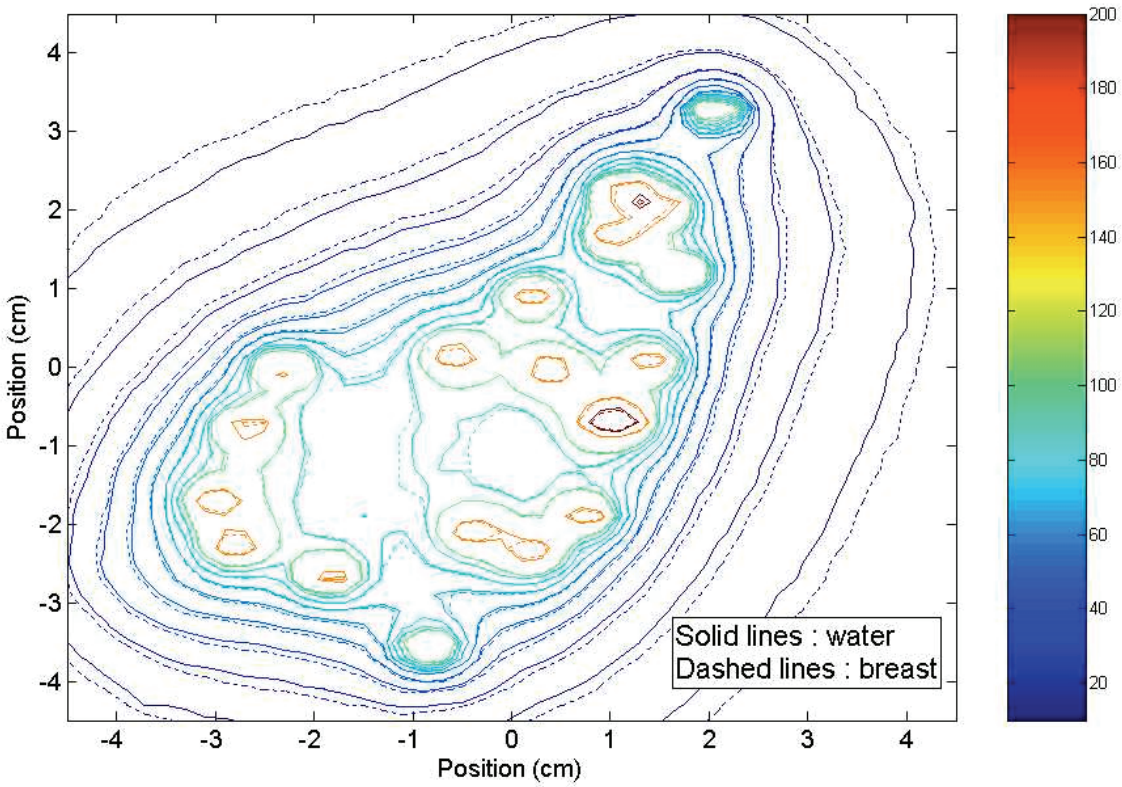


Figure 4.18 : Isodoses, normalised to centre for the breast implant in water and tissue.

#### 4.3.2.2. Tissue-Composition effect

Contrary to what is observed for the prostate implant, the DVH is left-shifted by ignoring the tissue-composition effect for a breast implant and the observed shift is very important. Hence, parameters such as the D90 are significantly underestimated by making the dosimetry in water instead of breast tissue. In that particular implant case, the difference on the D90 is 42%.

Ignoring the tissue-composition effect has a significant impact on dose distribution, as showed in figure 4.18. This figure shows the isodoses for the central slice for the breast implant in a breast tissue sphere. The isodoses are larger in breast tissue that what could be expected by calculating in water and the volume covered would be underestimated. Hence, a study of the breast tissue-composition effect on the DVH for healthy tissues and organs at risk and of the impact of such an underestimation would be interesting.

# Chapter 5. Conclusion and future work

For this work three different models were studied in order to see how the interseed and tissue-composition effects affects the dosimetry for LDR brachytherapy. Those models are the TG-43 calculation, calculated with Matlab using parameters determined with MC, the MC calculation in water and the MC calculation in realistic tissue. Our MC simulations were first validated by comparison with published TG-43 parameters and with TLD measurements.

We also made Gafchromic® EBT measurements and that dosimeter was validated for $^{125}$I LDR brachytherapy measurements by comparing calculations in water and tissue to check the perturbation introduced by the film and behind the film and by comparing the measurements Gafchromic measurements with TLD measurements and with MC calculations. A method to correct for dose-rate effect was also determined for LDR brachytherapy measurements.

Two effects were studied. First, we studied interseed effect for $^{125}$I seed model IBt. Comparisons were made with model 6711. We studied the impact on dose for one and two seeds. There is an attenuation due to the presence of seeds blocking the radiation. The interseed effect is generally less important for IBt than for 6711 because of the air in IBt. However, a small interseed effect, absent for 6711, can be observed for IBt seeds that are longitudinally aligned.

We also studied the variation of DVH due to interseed effect for realistic implants. The presence of seeds has the impact of left-shifting the DVH compared to the TG-43 calculations. The interseed effect generally becomes more important as the seed density augments, but particularities of a specific implant might have an impact. For instance, if the seeds are regrouped in one part of an implant (because of seed migration after the implantation for instance), the interseed effect might be more important than what would be expected due to the implant average density alone.

The second effect we studied is the tissue composition effect. Variation in radial dose function for one seed in different biological tissues was studied. It was also studied for diverse materials in order to associate potential phantom material to

tissues. It was determined that acrylic is a good substitute for breast tissue and that material was used in our experiments.

Variation in DVH due to tissue composition was also studied for a realistic prostate implant and for an hypothetical breast implant. The DVH in prostate tissue is left-shifted compare to the DVH in water, as expected according to literature. However, the DVH in breast tissue is right-shifted compare to the DVH in water the opposite of what happens in prostate tissue. Also, in breast implant, the isodoses gets larger in breast tissue compare to the isodoses in water so that the covered volume is larger due to tissue composition effect. Our study was made using $^{125}$I seeds even though breast implants are made with $^{103}$Pd seeds, but a similar effect can be expected with $^{103}$Pd since this effect is due to the tissue surrounding the seeds and not to the seeds themselves. The effect in breast implant for $^{103}$Pd would need to be studied in the future. Because of the smaller energy for $^{103}$Pd, the variation in photoelectric effect should be more important with that radionuclide and the tissue composition effect might be more significant. However, the dose gradient being steeper for $^{103}$Pd, so the effect might be slightly less important for $^{103}$Pd seeds, but this assumption would need to be studied.

Those two effects are ignored in TG-43-based dosimetry. For prostate implants, both effects are shifting the DVH to the left. Hence, dosimetry parameters like D90 and V200 are overestimated by TG-43 calculations.

For breast implants the interseed effect shifts the DVH to the left compared to the TG-43 DVH but the tissue-composition effect is shifting it back to the right. For the implant we studied, the right-shift is more important than the left-shift. Hence, the dosimetry parameters are underestimated a lot by the TG-43 calculation.

In the future, study of more realistic implants would be interesting, particularly for breast implants. To study the impact on treatment outcome of not considering the effects would also be useful. This would imply a study of the dose given to the tumor. In radiotherapy, we generally try to give a dose between 95% and 107% of the prescription dose to the tumor. In the implants we studied, an higher dose than that was given to the PTV, but not considering the tissue-composition effect augments the portion of the volume that gets a dose higher than 107% and a study of the

impact of that would have to be made. A study of the dose given to healthy tissues should also be made, particularly in view of the important underestimation of the dose given to tissues in the case of breast implant and in view of the more important volume covered since this means that dose would actually be given outside the PTV. A study for breast implant with a $^{103}$Pd seed would be interesting since it is that isotope that is used for that treatment. Finally, MC treatment planning could be developed, at first for post-implant study.

# References


1) R. Nath, L.L. Anderson, J.A. Meli, A.J. Olch, J.A. Stitt and J.F. Williamson, “Code of practice for brachytherapy physics : Report of the AAPM Radiation Therapy Committee Task Group No. 56,” Med. Phys. **24**(10), 1557-1598 (1997).
2) J.F. Williamson, M. Fatyga, N. Dogan, M. Hagan and D. Todor, “Brachytherapy in the Image-guided IMRT era,” Talk presented at the AAPM annual meeting, 2006.
3) www.americanbrachytherapy.org/aboutBrachytherapy/history.cfm.
4) F.M. Khan, “The physics of radiation therapy, 2nd edition” Williams and Wilkins, 1994.
5) www.prostatepointers.org/seedpods/brachy01.html.
6) www.uihealthcare.com/depts/med/urology/flocks/section5.html.
7) www.brachiterapia.it/ing.
8) www.radmed.osu.edu/myers-about-wgm.html.
9) E.B. Podgorsak, technical editor, “Radiation oncology physics : A handbook for teachers and students,” IAEA (2005), p.454.
10) www.msss.gouv.qc.ca.
11) S. Nag, D. Beyer, J. Friedland, P. Grimm and R. Nath, “American Brachytherapy Society (ABS) recommendations for transpineal permanent brachytherapy of prostate cancer,” Int. J. Radiation Oncology Biol. Phys. **44**(4), 789-799 (1999).
12) S. Nag, W. Bice, K. DeWyngaert, B. Prestidge, R. Stock and Y. Yu, “The American Brachytherapy Society recommendations for permanent prostate brachytherapy postimplant dosmetric analysis,” Int. J. Radiation Oncology Biol. Phys. **46**(1), 221-230 (2000).
13) S. Nag, J.P. Ciezki, R. Cormak, S. Dogget, K. DeWyngaert, G.K. Edmunson, R.G. Stock, N.N. Stone, Y. Yu and M.L. Zelefsky, “Intraoperative planning and evaluation of permanent prostate brachytherapy : Report of the American Brachytherapy Society,” Int. J. Radiation Oncology Biol. Phys. **51**(5), 1422-1430 (2001).

14) Y. Yu, L.L. Anderson, Z. Li, D.E. Mellenberg, R. Nath, M.C. Schell, F.M. Waterman, A. Wu and J.C. Blasko, "Permanent prostate seed implant brachytherapy : Report of the American Association of Physicists in Medicine Task Group No. 64," Med. Phys. **26**(10), 2054-2076 (1999).

15) R. Nath, L.L. Anderson, G. Luxton, K.A. Weaver and J.F. Williamson, "Dosimetry of interstitial brachytherapy sources : Recommandations of the AAPM Radiation Therapy Committee Task Group No. 43," Med. Phys. **22**(2), 209-234 (1995).

16) M.J. Rivard, B.M. Coursey, L.A. DeWerd, W.F. Hanson, M.S. Huq, G.S. Ibbott, M.G. Mitch, R. Nath and J.F. Williamson, "Update of AAPM Task Group No. 43 report : A revised AAPM protocol for brachytherapy dose calculation," Med. Phys. **31**(3), 633-674 (2004).

17) M.J. Rivard, W.M. Butler, L.A. DeWerd, M.S. Huq, G.S. Ibbott, A.S. Meigooni, C.S. Melhus, M.G. Mitch, R. Nath and J.F. Williamson, "Supplement to the update of the AAPM Task Group No. 43 Report," Med. Phys. **34**(6), 2187-2205 (2007).

18) B. Reniers, S. Vynkier and P. Scalliet, "Dosimetric study of the new Intersource-125 iodine seed," Med. Phys. **28**(11), 2285-2288 (2001).

19) B. Reniers, "The use of low energy photons in brachytherapy : Dosimetric and microdosimetric studies around $^{103}$Pd and $^{125}$I seeds," PhD thesis, Université Catholique de Louvain, faculté de médecine, Unité d'imagerie moléculaire et de radiothérapie expérimentale, 176p. (2005). And private comunication.

20) A. Meigooni, M. Yoe-Sein, A. Al Otoom, and K. Sowards, "Determination of the dosimetric characteristics of Intersource-125 iodine seed," Applied Radiation and isotopes, **56**(4), 589-599 (2002).

21) A.S. Meigooni, J.A. Meli, R. Nath., "Interseed effect for $^{125}$I Brachytherapy implant," Med. Phys. **19**(2), 633-674 (1992).

22) G.S. Burns and D.E.Raeside, "The accuracy of single-seed dose superposition for $^{125}$I implants," Med. Phys. **16**(4), 627-631 (1989).

23) O. Chibani, J.F. Williamson and Dorin Todor, "Dosimetric effects of seed anisotropy and interseed attenuation for $^{103}$Pd and $^{125}$I prostate implants," Med. Phys. **32**(8), 633-674 (2005).

24)P. Mobit and J. Badragan, “Dose perturbation in prostate seed implant brachytherapy with I-125,” Phys. Med Biol. **49**(14), 3171-3178 (2004).

25)J.-F. Carrier, L. Beaulieu, F. Therriault-Proulx and R. Roy, “Impact of interseed attenuation and tissue composition for permanent prostate implant,” Med. Phys. **33**(3), 595-604 (2006).

26)J.-F. Carrier, M. D’Amours, F. Verhaegen, B. Reniers, A.G. Martin, E. Vigneault and L. Beaulieu, “Postimplant dosimetry using a Monte Carlo dose calculation engine : A new clinical standard,” Int. J. Radiation Oncology Biol. Phys. **68**(4), 1190-1198 (2007).

27)J. Pérez-Calatayud, D. Granero and F. Ballester, “Phantom size in brachytherapy source dosimetric studies,” Med. Phys. **31**(7), 2075-2081 (2004).

28)www.physics.nist.gov/PhysRefData/contents.html

29)A.S. Meigooni, J.A. Meli and R. Nath, “A comparison of solid phantoms with water for dosimetry of $^{125}$I brachytherapy sources,” Med. Phys. **15**(5), 695-701 (1988).

30)Radiation Safety Information Computational Center, “ MCNP4C2 : Monte Carlo N particle transport code system,” RSICC Computer code collection, Oak Ridge laboratory (2001).

31)www.ibt4seeds.com.

32)A.F. McKinlay, “Thermo-luminescence dosimetry,” Medical Physics Handbooks, Adam Hilger Ltd, 170 p. (1981).

33)K.A. Weaver, “Response of LiF powder to $^{125}$I photons,” Med. Phys. **11**(6), 850-854 (1984).

34)K.A. Weaver, “Anisotropy functions of $^{125}$I and $^{192}$Ir seed sources,” Med.Phys. **25**(12), 2271-2278 (1998).

35)S.A. Dini, R.A. Koona, J.R. Ashbum, and A.S. Meigooni, “Dosimetric evaluation of Gafchromic® XR type T and XR type R films,” J. Appl. Clin. Med. Phys. **6**(1), 114-134 (2005).

36)S.-T.Chiu-Tsao, Y. Ho, R.Shankar, L. Wang and L.B. Harrison, “Energy dependence of response of new hi sensitivity radiochromic films for megavoltage and kilovoltage radiation energies,” Med. Phys. **32**(11), 3350-3354 (2005).

37)"Gafchromic® EBT, self developing film for radiotherapy dosimetry," www.ispcorp.com.

38)S. Devic, J. Seuntjens, E. Sham and E. B. Podgorsak, "Precise radiochromic film dosimetry using a flat-bed document scanner," Med. Phy. **32**(7), 2245-2253 (2005).

39)Ali, C. Costescu, M. Vicic, J.F. Dempsey and J.F. Williamson, "Dependence of radiochromic film optical density post-exposure kinetics on dose and dose fractionation," Med. Phys. **30**(8), 1958-1967 (2003).

40)"ICRU 44: Tissue Substitutes in Radiation Dosimetry and Measurement," International Commission on Radiation Units and Measurements, 1989.

41)W.S. Snyder, M.J. Cook, E.S. Nasset, L.R. Karhausen and I.H. Tipton, "Report of the task group on reference man," Technical report 23, International Commission on Radiological Protection (1974).

42)Gammex RMI, Middletown, WI, USA, www.gammex.com.

43)J.-F. Carrier, Centre Hospitalier Universitaire de Québec, Quebec, Canada, private communication

44)J.-P. Pignol, Sunnybrook Health Center, Toronto, Ontario, Canada, private communication